first generation AdV containing the switch unit inserted near the right end of the adenovirus genome (27) (denoted in this paper at the E4 position) and the target unit inserted in the E1 region. Since the adenovirus genome can be packaged into a capsid up to ~105% of, or 2 kb more than, the wild-type genome size (28), it was impossible to generate an AdV containing both the switch and the target units using a typical construction strategy because of over-sizing. Therefore, to shorten the total length of the units, an 'excisional-expression' structure was adopted for the target unit. Although a typical target unit for conditional expression possesses (in order) the potent promoter, *lox*P, a stuffer sequence, a second *lox*P, cDNA and polyadenylation sequences (poly(A)), the excisional-expression unit lacks a stuffer sequence and instead consists of (in order) the right *lox*P, dsRed cDNA, poly(A), EF1α promoter and the left *lox*P (Figure 1, Target unit on AxLR16EL-AC). Notably, the dsRed cDNA is located not downstream, but 'upstream' of the EF1α promoter and, therefore, dsRed expression is turned off in the initial structure because AFP promoter does not function in non-hepatocarcinoma cells. However, once the AdV infects a hepatocarcinoma cell, AFP promoter is turned on and Cre enzyme is produced. Consequently, the expression unit of dsRed—EF1α promoter with one *lox*P is 'excised' as a circular molecule (Figure 1, middle), and the dsRed cDNA is now located downstream of the EF1α promoter, turning its expression on. At the same time, an AdV genome with one *lox*P is produced (Figure 1, lower, AxL-AC).

To minimize the genome size of the double-unit AdV: (i) a 0.55-kb section of the E3 region was deleted (see 'Discussion' section). In addition (ii) the EF1α promoter was shortened from an original length of 2.1 kb to lengths of 1.6 and 1.4 kb (named 16EF and 14EF, respectively). Unexpectedly, both the 16EF and 14EF promoters showed higher activity levels than the original EF1α promoter (Figure 2). As well; (iii) the 0.6-kb rabbit β-globin poly(A) sequence was truncated to 0.3 kb up to *Nde*I site. In addition to the size limitation, the double-unit AdV possesses several features that enable a very strict specificity (see Discussion section). As an improvement, the poly(A) sequence of 137 nt derived from the SV40 early region (*Hpa*I-*Bam*HI) was added in front of the dsRed cDNA plus the right *lox*P on the target unit (Figure 1, upper) based on the results of the following experiments. We constructed three AdVs containing the *lac*Z DNA tagged with the nuclear localization signal [NLacZ (3)] and their structures are shown in Figure 3a. CV1 cells were infected with each of these AdVs at multiplicity of infection (MOI) of 50 and, three days later, the *lac*Z expression of the infected cells was detected with X-gal staining. When cells were infected with AxNZ containing promoterless NLacZ (Figure 3a, top), weak but significant background expression was observed in most of the cells (Figure 3b, lower left); such expression was not observed in mock-infected cells (Figure 3b, upper left). When cells were infected with AxLNZCAL containing an excisional expression unit lacking the poly(A) in front of the NLacZ plus *lox*P (Figure 3a, middle), significant expression was observed (Figure 3b, upper right) and the expression level was much higher than that using AxNZ (lower left). We speculate from these results that a weak cryptic promoter may present upstream of the NLacZ and be activated by the enhancer of CAG promoter downstream of the NLacZ. Nevertheless, using AxALNLZCAL containing the excisional expression unit possessing poly(A) in front of NLacZ DNA plus *lox*P (Figure 3a, bottom), the background expression was almost disappeared (Figure 3b, lower right). The result showed that the inserted poly(A) sequence effectively reduced the background expression. The results were confirmed in the transfection experiments using the cosmids containing the full-length AdV genome (data not shown). Finally, we attempted to construct two AdVs, AxLR16EL-AC (104.9% of wild-type adenovirus genome) and AxLR14EL-AC (104.4%) containing the 16EF and 14EF promoters, respectively. The genome sizes of both AdVs were under the size limit.

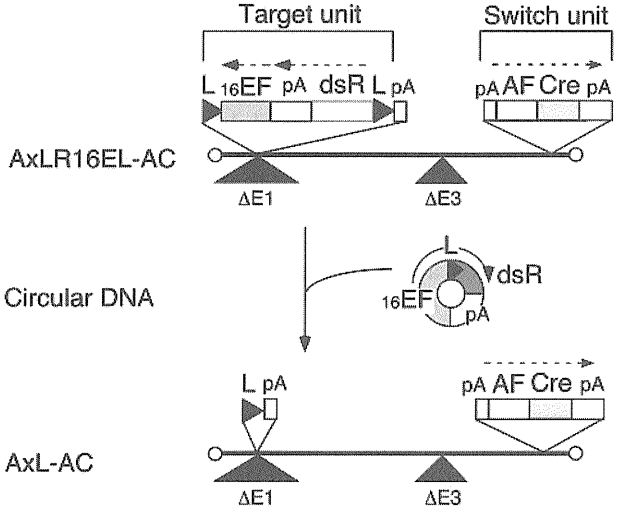

Figure 1. Structure of double-unit AdV and generation of expressing circular DNA. L, *lox*P; 16EF, shortened EF1α promoter; pA, poly(A) sequence; dsR, dsRed cDNA; AF, AFP promoter; Cre, nuclear localization signal-tagged Cre cDNA.

Leak expression of Cre both in *E. coli* and in 293 cells hampers the preparation of double-unit AdVs

Unexpectedly, during the construction of cosmids containing either AxLR16EL-AC or AxLR14EL-AC DNA (Figure 4a, dnCreRY –), we observed the co-generation of cosmids lacking the sequences between the two *lox*Ps (Figure 4b). The 2.5- and 2.7-kb bands (Figure 4c, lane 3) showed the presence of both cosmid DNA containing the AxL-AC genome and the excised circular DNA molecule, respectively. Judging from the intensities of the bands, the AxL-AC DNA accounted for ~15–20% of the midi-preparation (23) of *E. coli*. Thus, Cre must be expressed during cosmid preparation in *E. coli* DH5α despite the absence of an obvious *E. coli* promoter in the cosmid: the ampicillin promoter was present, but in the opposite orientation and ~20 kb away. Although the AxL-AC cosmid DNA was detected only faintly in the DNA of

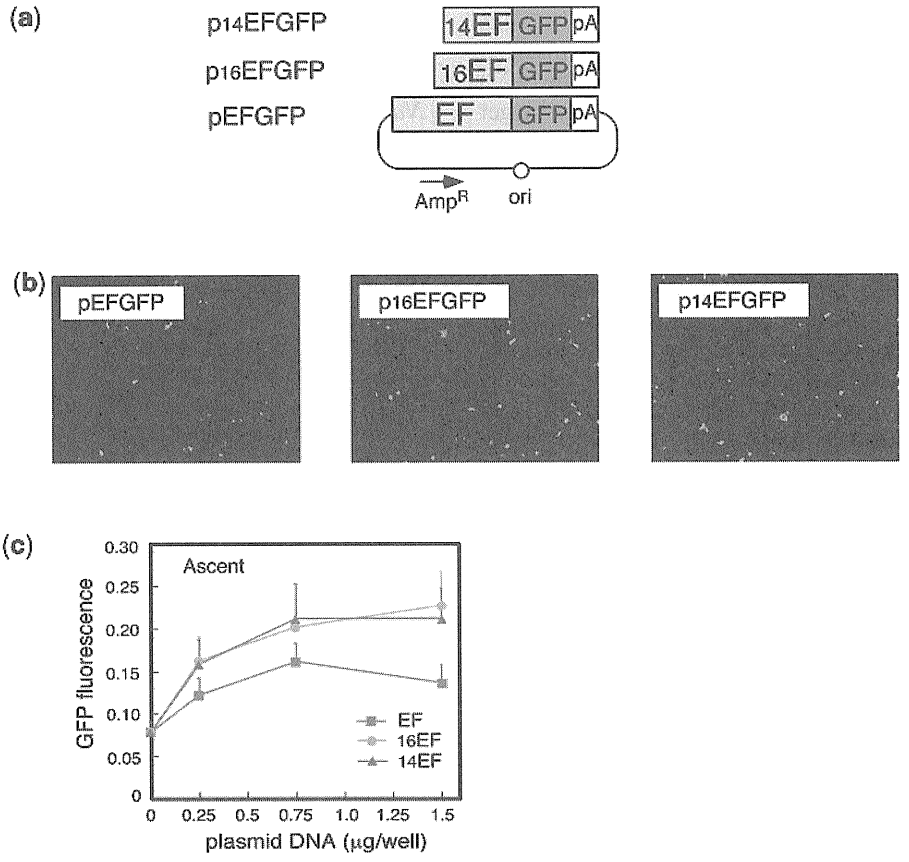

Figure 2. Expression of truncated EF1α promoter. (**a**) Structure of the plasmids expressing GFP under truncated EF1α promoter. The original EF1α promoter is 2.1-kb long. The 5′-end of 16EF was the *Ppu*MI site and that of 14EF was the *Blp*I site. (**b**) Images obtained using fluorescent microscopy. (**c**) Fluorescence measured using a fluoroscan plate reader. Vertical axis showed florescence in arbitrary unit; $n = 4$.

the mini-preparation (lane 2), it appeared to accumulate over time.

Furthermore, after the transfection of the cosmid DNA containing AxLR16EL-AC into 293 cells, all 12 of the viral clones that were generated were not the target virus, but apparently an AxL-AC virus. And three out of 18 viral clones derived from AxLR14EL-AC-containing cosmid DNA were mixtures of AxLR14EL-AC and AxL-AC viruses, while the other 15 clones were apparently pure AxL-AC virus (data not shown). These results showed that AFP promoter, which is thought to be inactive in non-hepatocellular 293 cells, certainly produced Cre in an amount sufficient to recombine the *lox*Ps on the AdV genome. This result probably occurred because even if the AFP promoter was strictly regulated, the AdV genome containing the switch unit of AFP promoter and Cre was amplified for 100 000 copies in one 293 cell and, consequently, an effective amount of Cre would be produced. Therefore, because of the leakage of Cre expression in both *E. coli* and 293 cells, double-unit vectors could not be prepared using conventional methods.

Successful suppression of leak expression of Cre using a dominant-negative of Cre and shRNA against Cre

To suppress the leak expression of Cre in *E. coli*, several dominant-negatives of Cre containing two amino acid mutations at the active center of Cre enzyme were constructed; dnCreRY, the dominant-negative that most efficiently suppressed Cre activity among those tested in co-transfection assays with a target plasmid, was then selected. Next, we constructed an expression unit producing dnCreRY under the control of the *trc* promoter of a *lac* operon system, and this unit was inserted into the cosmids containing AxLR16EL-AC and AxLR14EL-AC DNAs (Figure 4a, dnCreRY +). In the midi-preparation of this AxLR16EL-AC cosmid, neither the recombined AxL-AC-derived band nor the excised circular DNA molecule was detected with IPTG induction (Figure 4c, lane 7), showing that the production of dnCreRY successfully suppressed the leak expression of Cre in *E. coli*. Interestingly, since an apparent complete suppression was also observed without IPTG induction (lane 6), dnCreRY produced by the basal activity of the *trc* promoter was sufficient to suppress the leak expression of Cre effectively. Therefore, the problem of the leak expression of Cre in *E. coli* was solved.

To suppress the leak expression of Cre during AdV preparation in 293 cells, a plasmid expressing dnCreRY and a puromycin-resistant (PurR) gene (Figure 5a, upper) was transfected into 293 cells and the cell line 293dnCreRY8 was established; this cell line suppressed Cre activity the most efficiently. Virus clones were

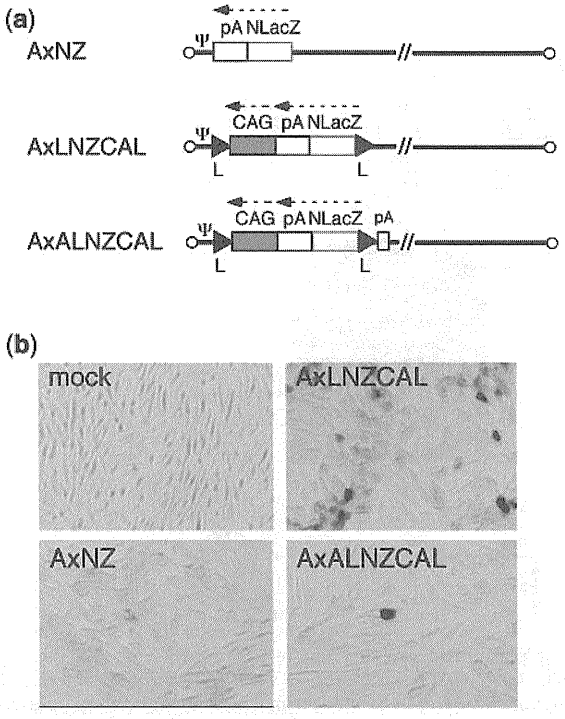

Figure 3. Suppression of the background expression by adding poly(A) sequence in front of *lac*Z DNA. (**a**) Structure of AdVs. (top) AxNZ contains the promoterless *lac*Z DNA; (middle) AxLNZCAL contains the excisional expression unit lacking poly(A) sequence in front of *lac*Z DNA plus right *lox*P; (bottom) AxALNZCAL contains that unit possessing poly(A) sequence in front of *lac*Z DNA plus right *lox*P. NlacZ, *lac*Z DNA tagged with NLS; Ψ, adenovirus packaging sequences; CAG, CAG promoter. The other representations are the same as in Figure 1. (**b**) Reduction of the 'background' expression observed using the promoterless *lac*Z DNA caused by addition of the poly(A) sequence. The infected CV1 cells were stained by X-gal. Very few dark-stained cells were observed in panels AxNZ (lower left) and AxALZCAL (lower right); the origin of these cells were unknown but possibly similar to those observed in Figure 7b and e.

obtained by transfecting linearized AxLR16EL-AC DNA, and the digestion of the viral genome with *Bmg*BI yielded a 1.8-kb band from an intact AxLR16EL-AC virus and a 1.4-kb band from a processed AxL-AC virus (Figure 5c). The 293dnCreRY8 cells did not produce pure AxLR16EL-AC virus, but instead produced mixtures of AxLR16EL-AC and AxL-AC (Figure 5a, lower, lanes 1, 3, 4 and 6) or mostly AxL-AC (lanes 2 and 5). Therefore, the suppression of Cre activity in the 293dnCreRY8 cells was not complete.

Meanwhile, several sh RNAs against Cre were constructed and screened, and shCreD was identified. Then, a plasmid expressing shCreD and PurR (Figure 5b, upper) was transfected into 293 cells, and the cell line 293shCreD13 was established. Unlike 293dnCreRY8, 293shCreD13 yielded mostly viral stocks of apparently pure AxLR16EL-AC virus (Figure 5b, lower, lanes 2, 3, 4 and 5), though some stocks were mixtures of both viruses (lanes 1 and 6). The AxLR16EL-AC virus in the apparently pure stocks was amplified in 293shCreD13 cells. To examine the 'leaky' expression level of Cre during the production of the double-unit vector in 293shCreD13 cells, an aliquot of AxLR16EL-AC viral stock was used to infect 293shCreD13 cells; then, to detect the viral genome, the total cell DNA was digested with *Bmg*BI. The 1.4-kb band produced by Cre recombination was not detected up to and including the third stock (data not shown) but, when the fourth stock purified using CsCl ultracentrifugation was examined, observed were the bands showing that the ratio of intact AxLR16EL-AC and 'leaked' AxL-AC was ~10:1 (Figure 5b, lower right). Of note, contamination with the AxL-AC virus does not cause any non-specific expression because Cre-processed AxL-AC virus does not contain an expression unit (Figure 1, bottom). An important point is that to prepare a double-unit AdV, the selection of an apparently

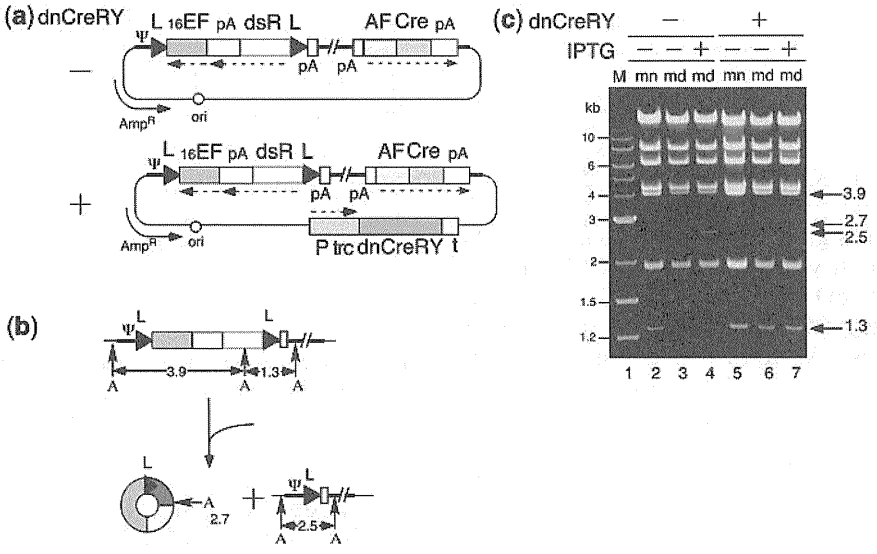

Figure 4. Leak expression of Cre in *E. coli*. Representations are the same as in Figure 1 unless otherwise stated. (**a**) Structure of cosmid generating double-unit AdV and expressing dnCreRY. Ψ, adenovirus packaging sequences; P trc, trc promoter; t, terminator. (**b**) Generation of Cre-processed molecules. A, *Ahd*I site. (**c**) Detection of Cre-processed molecules. M, 1-kb ladder marker; mn, mini-preparation; md; midi-preparation. The bands of 2.7 and 2.5 kb represent the generated circular DNA and Cre-processed DNA, respectively.

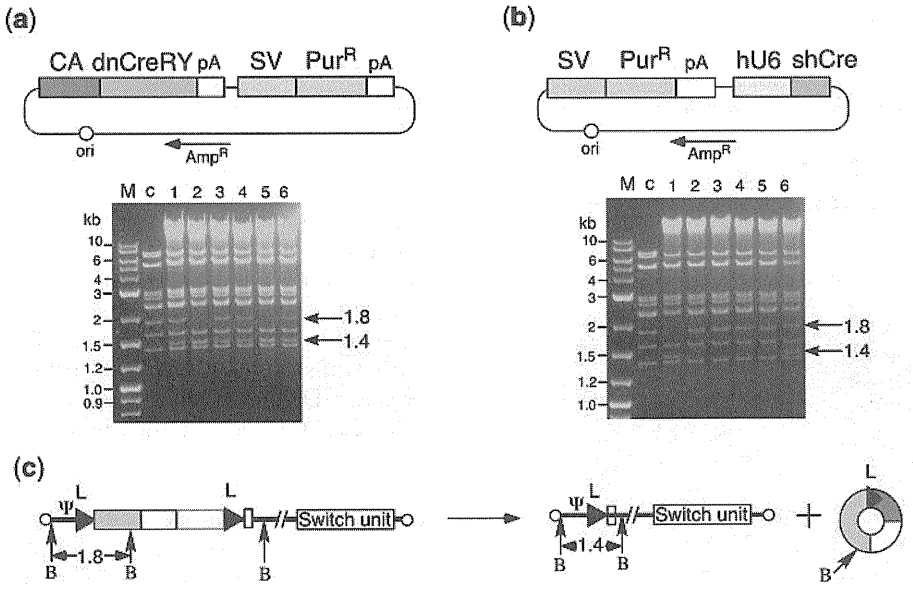

Figure 5. Establishment of 293 cell lines suppressing Cre activity. (**a**) Structure of plasmids expressing dnCreRY (upper) and DNA restriction pattern of double-unit viral clones produced in 293dnCreRY8 cells (lower). CA, CAG promoter; SV, SV40 early promoter; Pur^R, puromycin-resistant gene. The other representations are the same as in Figure 1. M, 1-kb ladder marker; c, restriction pattern of AxLR16EL-AC-containing cosmid DNA, presenting as a 1.8-kb band. (**b**) Structure of plasmids expressing shCre (upper) and DNA-restriction pattern of double-unit virus DNA of double-unit viral clones produced in 293shCreD13 cells (lower). hU6, human U6 promoter. P, purified/fourth stock was infected. The other representations are the same as in (a). (**c**) Generation of AxL-AC. B, *Bmg*BI site. The other representations are the same as in Figure 1. The presence or absence of circular 2.7-kb DNA was not clear in the gels of (a) and (b) because of the viral-derived bands of 2.9, 2.7 and 2.6 kb, but the circular DNA was hardly detected in the other experiment (data not shown). This result suggests that the production of the circular molecule occurs just after transfection and is consistent with the result that AxLR16EL-AC was stable up to the fourth stock.

Table 2. The viral titers of double-unit virus and the sprit viruses

Viruses[a]	Cells	Titers[b] ($TCID_{50}$)
AxLR16EL-AC	293shCreD13	1.1×10^{10}
AxLR16EL	Normal 293	4.7×10^{11}
Ax-AC	Normal 293	7.6×10^{10}

[a]The structure of AxLR16EL-AC is shown in Figure 1. The structures of split viruses, AxLR16EL and Ax-AC were shown in Figure 7a.
[b]Forth, purified viral stocks used in all experiments in this work.

pure first virus stock lacking AxL-AC as shown in Figure 5b, lower left, may be essential (see 'Discussion' section).

The 293shCreD13 cells grew well, similar to normal 293 cells, and the double-unit viruses were apparently able to proliferate in 293shCreD13 cells as well as normal E1-deficient AdV in 293 cells. Table 2 shows the titers of the double-unit virus AxLR16EL-AC produced in 293shCreD13 cells and of the split viruses shown in Figure 7a produced in normal 293 cells, all of which were used in this work. The titer of the double-unit virus was sufficiently high, though it was lower than those of the split viruses. One possible reason may be that the genome size of the former is near the upper limit. The AxLR14EL-AC virus was similarly prepared, and AxL-AC virus contamination was not detected in the third stock (data not shown).

The third viral stocks of double-unit virus without CsCl purification produced low but not negligible levels of non-specific dsRed expression when infected in HeLa cells (data not shown). Importantly, however, a viral preparation that was purified using a CsCl step gradient (22) did not produce any non-specific expression (see 'Discussion' section). Therefore, double-unit AdVs prepared in 293shCreD13 and purified using a CsCl step-gradient enabled the creation of viral stocks with a very strict specificity.

High-efficiency and very strict expression using double-unit AdV

The AxLR16EL-AC virus (at MOI of 5) was used to infect various cell types including HeLa (derived from non-liver carcinoma), SK-Hep1 (hepatocarcinoma-derived, non-producer of AFP), HuH-7 and HepG2 (hepatocarcinoma-derived producer of AFP). On day 3, high-level expressions of dsRed were observed in the infected HuH-7 and HepG2 cells (Figure 6h and k). Fluorescence-activated cell sorter (FACS) analyses showed that ~86 and 92% of these cells expressed detectable levels of dsRed, respectively (Figure 6i and l). In contrast, only one or two cells in a field of HeLa or SK-Hep1 cells expressed detectable levels of dsRed (Figure 6b and e), showing that the expression specificity of this vector was very strict. The FACS analyses confirmed that only 0.7 and 0.5% of the respective cells expressed detectable dsRed (Figure 6c and f). The results of dose-dependent experiments for all four cell lines confirmed the specificity of expression (Supplementary Figure S1).

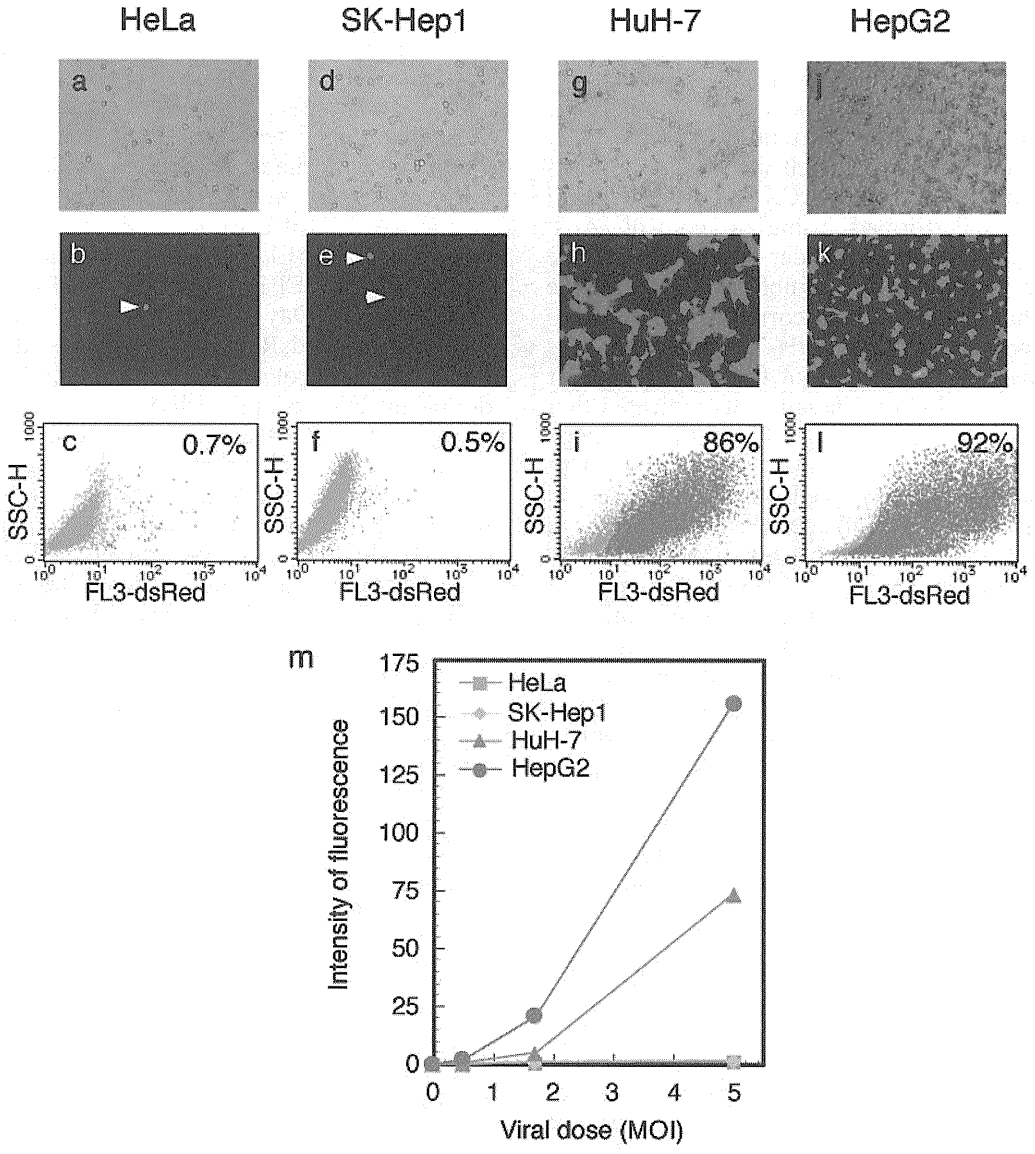

Figure 6. Specific and high-level expression of dsRed by AFP promoter using double-unit virus. Cells were infected with AxLR16EL-AC at MOI 5. (**a–c**) HeLa; (**d–f**) SK Hep-1; (**g–i**) HuH-7; (j, k and l) HepG2. (a, d, g and j) Phase-contrast microscopic views. (b, e, h and k) Images obtained using fluorescent microscopy. The arrow heads show exceptional cells with non-specific fluorescence. (c, f, i and l) FACS analysis of dsRed-expressing cells. SSC-H, side scattered light, high flow rate. (m) Dose responses of dsRed expression in the infected cells.

The dsRed expression was quantified using FACS by measuring the total sum of all cell fluorescence. The results showed that the ratio of the expressed mean fluorescence among the HeLa:SK-Hep1:HUH-7:HepG2 at MOI 5 in Figure 6c, f, i and l was 0.7:1:36.6:77.4, showing that the level of 'leaked' expression in the total cell population of AFP-negative cells compared with that in the AFP-positive cells was ~40 to 80 times less. The results of dose-dependent experiments are shown in Figure 6m. These results showed a very high expression and a strict specificity of this vector. Parallel to these FACS experiments, the transduction efficiency of the AdVs was measured by examining aliquots of all the four cell lines using real-time PCR as described in 'Materials and methods' section. The results indicated that the ratio of transduction efficiencies among HeLa, SK-Hep1, HuH-7 and HepG2 were 1.3:1:1.2:7.6, showing that the number of transduced AdV genomes present was almost the same for the first three cells. Therefore, these results confirmed very strict specificity of this vector for HeLa and SK-Hep1 cells. Meanwhile, HepG2 cells reproductively showed exceptionally high transduction efficiency. This seemed to be associated with the result that HepG2 showed much higher expression levels than HuH-7 cells (Figure 6m, at MOIs 1.7 and 5). Therefore, the very high expression level of HepG2 was partly explained by its exceptionally high transduction efficiency.

To examine the specificity of the double-unit vector, total RNA and DNA were extracted from AxLR16EL-AC-infected SK-Hep1 (AFP-negative) and HuH-7 (AFP-positive) cells. The amounts of expressed

dsRed RNAs and the transduced AdV genome were measured using real-time PCR as described in the Materials and methods section. The ratio of the dsRed RNA level corrected according to the transduced AdV genome between the two cell lines was calculated. The result showed that the dsRed RNA ratio of HuH-7 and SK-Hep1was 42.0:1, correlating well with the quantification of dsRed expression using FACS analyses. Identical experiments were performed using a control AdV AxCAdsRed expressing dsRed under the control of the CAG promoter instead of the double-unit vector. The result showed that the RNA ratio corrected according to the viral DNA amount between HuH-7 and SK-Hep1was 1.38:1, indicating that the activity of the CAG promoter was similar in both cell lines. These results indicated that the 'leak' level of the double-unit vector in the SK-Hep1 cells, compared with that in the HuH-7 cells, was ~1/40th of the expression level of HuH-7 cells (or 1/30th, based on of the CAG promoter control), demonstrating that the background level of double-unit vector in AFP-negative cells was again very low.

To examine the effect of combining the switch unit and the target unit into a single genome, we newly constructed two AdVs: AxLR16EL, containing only the target unit (Figure 7a, first), and Ax-AC, containing the switch unit at the E4 position (Figure 7a, second), as in AxLR16EL-AC. Then, the expression of the double-unit vector (AxLR16EL-AC) and the double infection of split viruses containing the excisional expression unit (AxLR16EL + Ax1AC) was examined using dsRed fluorescence. The double-unit vector showed a much higher fluorescence level than the double-infection method, as observed under a fluorescent microscope (Figure 7b). And the quantitative measurement of dsRed fluorescence showed that the former method produced 3.3-fold more dsRed protein than the latter method using an MOI of 13 (Figure 7c). The reason that the expression level was higher than that of the split viruses appears to be not only because the amount of the target virus was one half of the same total dose of the viruses, but also because in many cells, the split two vectors were not infected simultaneously or did not produce a sufficient amount of Cre during five days.

The steady-state levels of expressed dsRed RNA measured using real-time PCR in HuH-7 cells were compared with the direct expression under the control of AFP promoter (AxA2AdsR, Figure 7a), a double-unit vector (AxLR16EL-AC), a double-infection of split viruses (AxLR16EL + Ax-AC), and the expression under the control of EF1α promoter (AxEFdsR, Figure 7a) (Table 3). On Day 3, the double-unit vector expressed ~40-fold more dsRed RNA than the direct expression under the control of AFP promoter. Meanwhile, the double infection of split viruses (AxLR16EL + Ax-AC) expressed dsRed RNA at a level only 1/4th of that expressed by the double-unit vector, confirming the expression results (Figure 7c). Because the dsRed RNA expressed by the EF1α promoter (AxEFdsR) in HuH-7 cells was 480-fold higher than the direct expression of AFP promoter, the double-unit vector utilized ~1/10th of the EF1α promoter activity on day 3. However, on day 4, the

Table 3. Steady-state levels of expressed dsRed RNA in HuH-7 cells

AdV[a]	Ratio[b]
AxA2AdsR	1
AxLR16EL-AC	41
AxLR16EL + Ax-AC	10
AxEFdsR	480
AxLR16EL-AC (day 4)	91

Each experiment was performed twice to confirm the reproducibility; typical data are shown. The genome structures of the above viruses are shown in Figures 1 and 7a.
[a]HuH-7 cells were infected with each AdV at a MOI of 30. In the double infection, an MOI 15 of each virus was used.
[b]For each condition, the expressed dsRed RNA measured using real-time PCR was divided by the value obtained using the AxA2AdsR virus.

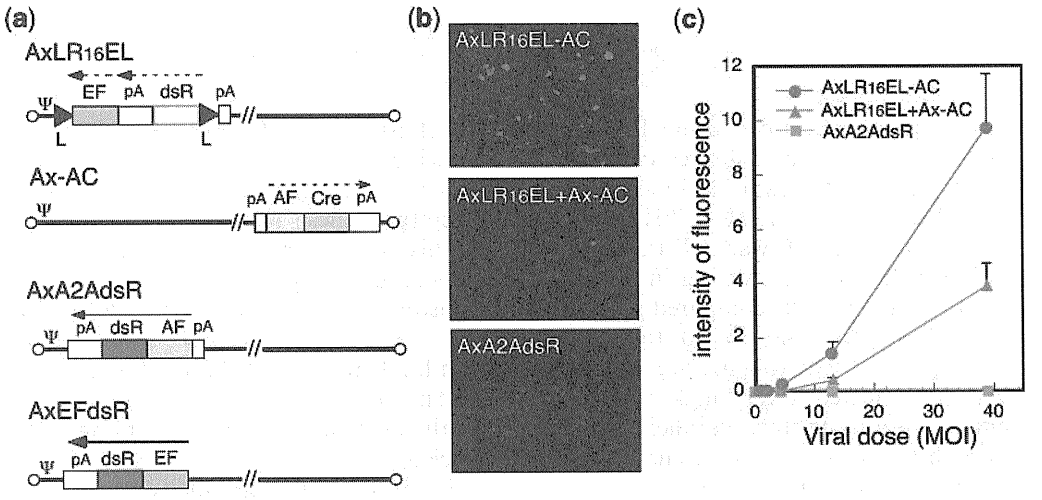

Figure 7. Simultaneous excisional expression in HuH-7 cells using double-infection method. (**a**) Structure of AdVs. The representations are the same as in Figure 1. (**b**) Images obtained using fluorescent microscopy. (**c**) Fluorescence measured using a fluoroscan plate reader.

expression of dsRed RNA reached ~90-fold when using the double-unit vector (Table 3); because such an increase in expression on later days was often observed in other double-unit experiments (data not shown), this result can likely be explained by the weak AFP promoter, since the very small amount of expressed Cre likely required a long time to process the target unit.

DISCUSSION

We developed a 'double-unit' AdV bearing an 'excisional-expression' structure and established a preparation method for this AdV. The AdV showed a high level of expression of the target gene under the control of a tissue/cancer-specific promoter, maintaining a very strict specificity. We observed that (i) because the vector was a first-generation AdV, it could be prepared on a large-scale without difficulty, and (ii) although a leak in Cre expression was observed during its preparation in *E. coli* and 293 cells, both problems were solved using a dominant-negative of Cre, dnCreRY, and an shRNA against Cre, shCreD, respectively. The complete suppression of Cre expression in 293 cells has been especially problematic, since AdV genome replication produces up to ~100 000 genome copies in each 293 cell. The key step in the production of the double-unit AdV was the selection of a clone lacking the AxL-AC virus (Figure 5b, lower left). Our results showed that severe AxL-AC generation caused by the leaky expression of Cre occurred 'before' the selection of a clone lacking the AxL-AC virus and that once such a clone was obtained, problematic deletion caused by 'leaked' Cre was not observed during the second to fourth production steps. Therefore, for the production of double-unit AdV even using 293shCreD13 cells, popular AdV-production protocols producing a pool of AdVs after transfection cannot be used.

As stated in the 'Introduction' section, this vector system is obviously superior to the 'double-infection' method (3); in the latter system, two viruses must be simultaneously transduced into a single cell for expression, and the infection of only one virus in a single cell is useless but causes similar viral toxic effects. Therefore, this new system will be particularly useful under diluted conditions, such as in animal experiments for basic research (unpublished data) as well as human gene therapy. Here, AFP promoter was used as one example, but obviously any tissue/cancer-specific promoter can be used. We intentionally did not adopt a CMV or CAG promoter, but instead used an EF1α promoter as a potent and non-specific promoter in the target unit because we have previously shown that the EF1α promoter hardly induces any inflammation as a result of AdV infection in an *in vivo* experiment, since no detectable induction of viral pIX production occurs (29). One report describing 'excisional expression' where a gene product was expressed only after excision by Cre from a Cre-excised circular molecule as described here has been previously published (30), but the purpose of this previous report was entirely different from that of the present work because the objective of the previous study was to examine persistent expression as a circular replicon using EB-viral oriP and used a double infection system using Cre-expressing AdV. Also, Yant *et al.* (31) reported another type of the 'excisional expression', where intron-containing transgenes were split and thus remained inactive until an FLP-mediated circularization restored the correct reading frame. The excision of an expression unit from the AdV genome by Cre or FLP has occasionally been reported (for examples, 32–34).

We observed a 'leak' in the expression level of the double-unit vector in an AFP-negative cell population amounting to ~1/40th of the expression level in HuH-7 cells measured using FACS as the total sum of all cell florescence, as stated in the Results section. While this level was very low, it was similar to the activity of the authentic AFP promoter in HuH-7 cells (Table 3). However, in AFP-negative cells infected with a double-unit virus, a small number of 'bright cells' highly expressing dsRed (Figure 6b, e and c, f) were present, increasing the apparent 'leaked' expression level.

Importantly, the specificity of the tissue/cancer promoter in this vector was very strictly maintained for a number of reasons. (i) Because the potent EF1α promoter in the target unit is present 'downstream' of the cDNA (Figure 1), an expression leak of the cDNA via this promoter is not possible until the promoter is translocated in front of the target cDNA by *lox*P recombination and circularization. (ii) The *lox*P-combined virus AxL-AC generated during the preparation of the double-unit virus does not contain an expression unit and hence does not cause non-specific expression. In contrast, the double-infection method always generates some stuffer-less, *lox*P-combined virus that causes non-specific expression because a small amount of such virus is generated even without Cre gene in AdV preparations, possibly through the homologous recombination of ~50 nt consisting of *lox*Ps and its surrounding sequences (3). (iii) Though conventional viral stock contains a small amount of circular DNA expressing the target gene and causing non-specific expression, it can be completely removed using a CsCl step gradient (22), since the DNA is much heavier than the virus particle. We previously observed that a DNA molecule in the viral stock can be 'transfected' into infected cells (35). (iv) The tissue-/cancer-specific promoter is inserted at the E4 position and is located farthest from the enhancer of a potent and non-specific EF1α promoter inserted at the E1-insertion site present near the left end of the genome. Therefore, the enhancer effect of the EF1α promoter on the specific AFP promoter is minimized. (v) A poly(A) sequence in front of the specific AFP promoter in the switch unit (Figure 1, upper right) suppresses non-specific transcription through a cryptic promoter present upstream of the specific promoter (3). And finally (vi) another poly(A) sequence in front of the *lox*P-cDNA in the target unit (Figure 1, upper left, and Figure 3) efficiently reduce the non-specific expression of cDNA probably caused by upstream cryptic promoters. We cannot argue whether the double-unit system is better in selectivity and less 'leaky' than the

authentic AFP promoter used here; for such conclusion further studies are needed using a more sensitive reporter system. However, because of these reasons above, the double-unit vector copes with high-level expression and strict specificity.

The total length of the AdV genome used in this method should not be more than ~38 kb (28). This means that the maximum length of a specific promoter plus target cDNA in this vector system with *Bsu*36I-*Blp*I E3 deletion (see below) should be 3.9 kb when the 14EF1α promoter is used and 4.5 kb when the 0.8-kb CMV promoter is used. This limitation of the length does not cause a problem in most cases. For example, because the AFP promoter used here is 2.2 kb in length, herpes thymidine-kinase cDNA (1.2 kb) or luciferase cDNA (1.7 kb) can be inserted; in fact, we constructed a double-unit AdV containing both AFP promoter and the thymidine-kinase gene, and animal experiments examining suicide-gene therapy are presently underway.

The problem of the genome length limitation can be solved using an AdV with a larger deletion in the E3 and E4 region. In the present study, AxLR14EL-AC and AxLR16EL-AC carried a *Bsu*36I-*Blp*I E3 deletion of 2433 bp, corresponding to 28 342–30 775-nt positions in the adenovirus type 5 map. The E3 region was 555-bp shorter than the *Xba*I-*Xba*I deleted E3 (21,27) and 252-bp longer than the *Bgl*II-*Bgl*II deleted E3 (36,37). We avoided using the *Bgl*II-*Bgl*II deleted E3 because L4 mRNAs of this AdV miss the L4 poly(A) sequences but use E3 poly(A) sequences, while *Xba*I-*Xba*I and *Bsu*36I-*Bpl*I deleted E3 both use the authentic L4 poly(A) sequences. Since an even shorter E3 region (27 865–30 995 nt) (36,38) and an E4 deletion (32 825–35 640 nt) (38) have been reported, the 3.9-kb limitation of the total lengths of a specific promoter plus cDNA when using AxLR14EL-AC could be enlarged up to 7.4 kb, if these vector constructs could be used.

Interestingly, Huyn *et al.* (39) recently reported an apparently related but different AdV system where, as the switch unit, a cancer-specific promoter produces a Gal4-VP16 fusion protein and, as the target unit, a Gal4-binding domain plus a CMV minimal promoter is used. They claimed that their method might be useful for visualizing cancer metastasis. A comparison of our vector with theirs would be difficult because they confirmed promoter specificity only in transfection experiments and because a cancer-specific promoter different from ours was used. Since our vector was developed with the goals of not only achieving a high expression level, but also of achieving a very low background in applications and ensuring the safety of gene therapy, the purposes of these studies are clearly different.

The method described here was totally different from that used for cancer-specific, replication-competent AdVs (for reviews, see references 40,41) in the field of cancer gene therapy. Although these AdVs use cancer-specific promoters, the adenoviruses replicate in the target cells and produce damaging effects through adenovirus gene expression in the target and surrounding cells. Although it has been reported that replication of E1-dereted AdV can be detected by Southern hybridization technique in HeLa cells at a higher MOI (42) and in other certain cells two weeks after infection (43), the replication level seemed too low to influence on the results described here.

The AdV system described here is probably useful for studying the function of a gene product in a specific tissue or organ. In any given tissue, several different sorts of cells are present: for example, neurons, glia cells and vascular endothelial cells are simultaneously present in neural tissue. Thus, this vector would be useful for expressing a gene selectively and efficiently in only one type of cell using a cell-specific promoter. This activity could enable novel, specific and effective therapies to be eveloped in the field of cancer gene therapy, and this strategy is now being tested. Furthermore, the application of this vector could be extended to include those where a high expression level and a rigid specificity are necessary.

The vector described here will be useful for many researchers using tissue/cancer-specific promoters. Plasmids suppressing Cre activity, cosmid cassettes for the construction of double-unit AdV containing *trc*-dnCreRY, and the 293 cell lines 293dnCreRY8 and 293shCreD13 are available from Riken Bioresource Bank (http://www.brc.riken.go.jp/) or in collaboration basis.

SUPPLEMENTARY DATA

Supplementary data are available at NAR Online.

ACKNOWLEDGMENTS

The authors thank Ms E. Kondo for her excellent secretarial assistance.

FUNDING

This work was supported by the Grant in Aid for Scientific Research on Priority Areas from Ministry of Education, Culture, Sports, Science and Technology, Japan (to I.S.). Funding for open access charge: Institute of Medical Science, University of Tokyo.

Conflict of interest statement. None declared.

REFFERENCES

1. Niwa,H., Yamamura,K. and Miyazaki,J. (1991) Efficient selection for high-expression transfectants with a novel eukaryotic vector. *Gene*, **108**, 193–199.
2. Kim,D.W., Uetsuki,T., Kaziro,Y., Yamaguchi,N. and Sugano,S. (1990) Use of the human elongation factor 1 alpha promoter as a versatile and efficient expression system. *Gene*, **91**, 217–223.
3. Sato,Y., Tanaka,K., Lee,G., Kanegae,Y., Sakai,Y., Kaneko,S., Nakabayashi,H., Tamaoki,T. and Saito,I. (1998) Enhanced and specific gene expression via tissue-specific production of Cre recombinase using adenovirus vector. *Biochem. Biophys. Res. Commun.*, **244**, 455–462.
4. Wilson,C., Bellen,H.J. and Gehring,W.J. (1990) Position effects on eukaryotic gene expression. *Annu. Rev. Cell Biol.*, **6**, 679–714.

5. Giraldo,P. and Montoliu,L. (2001) Size matters: use of YACs, BACs and PACs in transgenic animals. *Transgenic Res.*, **10**, 83–103.
6. Kijima,T., Osaki,T., Nishino,K., Kumagai,T., Funakoshi,T., Goto,H., Tachibana,I., Tanio,Y. and Kishimoto,T. (1999) Application of the Cre recombinase/*lox*P system further enhances antitumor effects in cell type-specific gene therapy against carcinoembryonic antigen-producing cancer. *Cancer Res.*, **59**, 4906–4911.
7. Ueda,K., Iwahashi,M., Nakamori,M., Nakamura,M., Yamaue,H. and Tanimura,H. (2000) Enhanced selective gene expression by adenovirus vector using Cre/*lox*P regulation system for human carcinoembryonic antigen-producing carcinoma. *Oncology*, **59**, 255–265.
8. Ueda,K., Iwahashi,M., Nakamori,M., Nakamura,M., Matsuura,I., Yamaue,H. and Tanimura,H. (2001) Carcinoembryonic antigen-specific suicide gene therapy of cytosine deaminase/5-fluorocytosine enhanced by the cre/*lox*P system in the orthotopic gastric carcinoma model. *Cancer Res.*, **61**, 6158–6162.
9. Goto,H., Osaki,T., Kijima,T., Nishino,K., Kumagai,T., Funakoshi,T., Kimura,H., Takeda,Y., Yoneda,T., Tachibana,I. *et al.* (2001) Gene therapy utilizing the Cre/*lox*P system selectively suppresses tumor growth of disseminated carcinoembryonic antigen-producing cancer cells. *Int. J. Cancer*, **94**, 414–419.
10. Ueda,K., Iwahashi,M., Nakamori,M., Nakamura,M., Matsuura,I., Ojima,T. and Yamaue,H. (2003) Improvement of carcinoembryonic antigen-specific prodrug gene therapy for experimental colon cancer. *Surgery*, **133**, 309–317.
11. Nagayama,Y., Nishihara,E., Iitaka,M., Namba,H., Yamashita,S. and Niwa,M. (1999) Enhanced efficacy of transcriptionally targeted suicide gene/prodrug therapy for thyroid carcinoma with the Cre-*lox*P system. *Cancer Res.*, **59**, 3049–3052.
12. Sakai,Y., Kaneko,S., Sato,Y., Kanegae,Y., Tamaoki,T., Saito,I. and Kobayashi,K. (2001) Gene therapy for hepatocellular carcinoma using two recombinant adenovirus vectors with alpha-fetoprotein promoter and Cre/*lox* P system. *J. Virol. Methods*, **92**, 5–17.
13. Yoshimura,I., Ikegami,S., Suzuki,S., Tadakuma,T. and Hayakawa,M. (2002) Adenovirus mediated prostate specific enzyme prodrug gene therapy using prostate specific antigen promoter enhanced by the Cre-*lox*P system. *J. Urol.*, **168**, 2659–2664.
14. Maeda,M., Namikawa,K., Kobayashi,I., Ohba,N., Takahara,Y., Kadono,C., Tanaka,A. and Kiyama,H. (2006) Targeted gene therapy toward astrocytoma using a Cre/*lox*P-based adenovirus system. *Brain Res.*, **1081**, 34–43.
15. Namikawa,K., Murakami,K., Okamoto,T., Okado,H. and Kiyama,H. (2006) Efficient generation of recombinant adenoviruses using adenovirus DNA-terminal protein complex and a cosmid bearing the full-length virus genome. *Gene Ther.*, **13**, 1244–1250.
16. Graham,F.L., Smiley,J., Russell,W.C. and Nairn,R. (1977) Characteristics of a human cell line transformed by DNA from human adenovirus type 5. *J. Gen. Virol.*, **36**, 59–74.
17. Aden,D.P., Fogel,A., Plotkin,S., Damjanov,I. and Knowles,B.B. (1979) Controlled synthesis of HBsAg in a differentiated human liver carcinoma-derived cell line. *Nature*, **282**, 615–616.
18. Nakabayashi,H., Taketa,K., Miyano,K., Yamane,T. and Sato,J. (1982) Growth of human hepatoma cells lines with differentiated functions in chemically defined medium. *Cancer Res.*, **42**, 3858–3863.
19. Fogh,J., Fogh,J.M. and Orfeo,T. (1977) One hundred and twenty-seven cultured human tumor cell lines producing tumors in nude mice. *J. Natl Cancer Inst.*, **59**, 221–226.
20. Ido,A., Nakata,K., Kato,Y., Nakao,K., Murata,K., Fujita,M., Ishii,N., Tamaoki,T., Shiku,H. and Nagataki,S. (1995) Gene therapy for hepatoma cells using a retrovirus vector carrying herpes simplex virus thymidine kinase gene under the control of human alpha-fetoprotein gene promoter. *Cancer Res.*, **55**, 3105–3109.
21. Fukuda,H., Terashima,M., Koshikawa,M., Kanegae,Y. and Saito,I. (2006) Possible mechanism of adenovirus generation from a cloned viral genome tagged with nucleotides at its ends. *Microbiol. Immunol.*, **50**, 643–654.
22. Kanegae,Y., Makimura,M. and Saito,I. (1994) A simple and efficient method for purification of infectious recombinant adenovirus. *Jpn. J. Med. Sci. Biol.*, **47**, 157–166.
23. Sambrook,J. and Russell. (1989) *Molecular Cloning: A Laboratory Manual*, Vol. 1, 3rd edn. Cold Spring Harbor Laboratory Press, Cold Spring Harbor, NY.
24. Kanegae,Y., Takamori,K., Sato,Y., Lee,G., Nakai,M. and Saito,I. (1996) Efficient gene activation system on mammalian cell chromosomes using recombinant adenovirus producing Cre recombinase. *Gene*, **181**, 207–212.
25. Saito,I., Oya,Y., Yamamoto,K., Yuasa,T. and Shimojo,H. (1985) Construction of nondefective adenovirus type 5 bearing a 2.8-kilobase hepatitis B virus DNA near the right end of its genome. *J. Virol.*, **54**, 711–719.
26. Kondo,S., Takata,Y., Nakano,M., Saito,I. and Kanegae,Y. (2009) Activities of various FLP recombinases expressed by adenovirus in mammalian cells. *J. Molec. Biol.*, **390**, 221–230.
27. Miyake,S., Makimura,M., Kanegae,Y., Harada,S., Sato,Y., Takamori,K., Tokuda,C. and Saito,I. (1996) Efficient generation of recombinant adenoviruses using adenovirus DNA-terminal protein complex and a cosmid bearing the full-length virus genome. *Proc. Natl Acad. Sci. USA*, **93**, 1320–1324.
28. Bett,A.J., Prevec,L. and Graham,F.L. (1993) Packaging capacity and stability of human adenovirus type 5 vectors. *J. Virol.*, **67**, 5911–5921.
29. Nakai,M., Komiya,K., Murata,M., Kimura,T., Kanaoka,M., Kanegae,Y. and Saito,I. (2007) Expression of pIX gene induced by transgene promoter: possible cause of host immune response in first-generation adenoviral vectors. *Hum. Gene Ther.*, **18**, 925–936.
30. Leblois,H., Roche,C., Di Falco,N., Orsini,C., Yeh,P. and Perricaudet,M. (2000) Stable transduction of actively dividing cells via a novel adenoviral/episomal vector. *Mol. Ther.*, **1**, 314–322.
31. Yant,S.R., Ehrhardt,A., Mikkelsen,J.G., Meuse,L., Pham,T. and Kay,M.A. (2002) Transposition from a gutless adeno-transposon vector stabilizes transgene expression in vivo. *Nat. Biotechnol.*, **20**, 999–1005.
32. Gil,J.S., Gallaher,S.D. and Berk,A.J. (2010) Delivery of an EBV episome by a self-circularizing helper-dependent adenovirus: long-term transgene expression in immunocompetent mice. *Gene Ther.*, doi:10.1038/gt.2010.75.
33. Dorigo,O., Gil,J.S., Gallaher,S.D., Tan,B.T., Castro,M.G., Lowenstein,P.R., Calos,M.P. and Berk,A.J. (2004) Development of a novel helper-dependent adenovirus-Epstein-Barr virus hybrid system for the stable transformation of mammalian cells. *J. Virol.*, **78**, 6556–6566.
34. Lee,J.H., Yi,S.M., Anderson,M.E., Berger,K.L., Welsh,M.J., Klingelhutz,A.J. and Ozbun,M.A. (2004) Propagation of infectious human papillomavirus type 16 by using an adenovirus and Cre/*Lox*P mechanism. *Proc. Natl Acad. Sci. USA*, **101**, 2094–2099.
35. Nakano,M., Odaka,K., Takahashi,Y., Ishimura,M., Saito,I. and Kanegae,Y. (2005) Production of viral vectors using recombinase-mediated cassette exchange. *Nucleic Acids Res.*, **33**, e76.
36. Bett,A.J., Haddara,W., Prevec,L. and Graham,F.L. (1994) An efficient and flexible system for construction of adenovirus vectors with insertions or deletions in early regions 1 and 3. *Proc. Natl Acad. Sci. USA*, **91**, 8802–8806.
37. Mizuguchi,H. and Kay,M.A. (1998) Efficient construction of a recombinant adenovirus vector by an improved in vitro ligation method. *Hum. Gene Ther.*, **9**, 2577–2583.
38. Mizuguchi,H. and Kay,M.A. (1999) A simple method for constructing E1- and E1/E4-deleted recombinant adenoviral vectors. *Hum. Gene Ther.*, **10**, 2013–2017.
39. Huyn,S.T., Burton,J.B., Sato,M., Carey,M., Gambhir,S.S. and Wu,L. (2009) A potent, imaging adenoviral vector driven by the cancer-selective mucin-1 promoter that targets breast cancer metastasis. *Clin. Cancer Res.*, **15**, 3126–3134.

40. Toth,K., Dhar,D. and Wold,W.S. (2010) Oncolytic (replication-competent) adenoviruses as anticancer agents. *Expert Opin. Biol. Ther.*, **10**, 353–368.
41. Mathis,J.M., Stoff-Khalili,M.A. and Curiel,D.T. (2005) Oncolytic adenoviruses – selective retargeting to tumor cells. *Oncogene*, **24**, 7775–7791.
42. Steinwaerder,D.S., Carlson,C.A. and Lieber,A. (2001) Human papilloma virus E6 and E7 proteins support DNA replication of adenoviruses deleted for the E1A and E1B genes. *Mol. Ther.*, **4**, 211–216.
43. Ghosh,S. and Duigou,G.J. (2005) Decreased replication ability of D1-deleted adenoviruses correlates with increased brain tumor malignancy. *Cancer Res.*, **65**, 8936–8943.

Research Article

EASL EUROPEAN ASSOCIATION FOR THE STUDY OF THE LIVER | JOURNAL OF HEPATOLOGY

Pathogenesis of lipid metabolism disorder in hepatitis C: Polyunsaturated fatty acids counteract lipid alterations induced by the core protein

Hideyuki Miyoshi[1], Kyoji Moriya[1], Takeya Tsutsumi[1], Seiko Shinzawa[1], Hajime Fujie[1], Yoshizumi Shintani[1], Hidetake Fujinaga[1], Koji Goto[1], Toru Todoroki[2], Tetsuro Suzuki[3], Tatsuo Miyamura[3], Yoshiharu Matsuura[4], Hiroshi Yotsuyanagi[1], Kazuhiko Koike[1,*]

[1]*Department of Internal Medicine, Graduate School of Medicine, University of Tokyo, Tokyo, Japan;* [2]*Department of Laboratory Medicine, Keio University School of Medicine, Tokyo, Japan;* [3]*Department of Virology II, National Institute of Infectious Diseases, Tokyo, Japan;* [4]*Department of Molecular Virology, Research Institute for Microbial Diseases, Osaka University, Osaka, Japan*

Background & Aims: Disturbance in lipid metabolism is one of the features of chronic hepatitis C, being a crucial determinant of the progression of liver fibrosis. Experimental studies have revealed that the core protein of hepatitis C virus (HCV) induces steatosis.

Methods: The activities of fatty acid metabolizing enzymes were determined by analyzing the fatty acid compositions in HepG2 cells with or without core protein expression.

Results: There was a marked accumulation of triglycerides in core-expressing HepG2 cells. While the oleic/stearic acid (18:1/18:0) and palmitoleic/palmitic acid ratio (16:1/16:0) were comparable in both the core-expressing and the control cells, there was a marked accumulation of downstream product, 5,8,11-eicosatrienoic acid (20:3(n-9)) in the core-expressing HepG2 cells. The addition of eicosatetraynoic acid, which inhibits delta-6 desaturase activity which is inherently high in HepG2 cells, led to a marked accumulation of oleic and palmitoleic acids in the core-expressing cells, showing that delta-9 desaturase was activated by the core protein. Eicosapentaenoic acid (20:5(n-3)) or arachidonic acid (20:4(n-6)) administration significantly decreased delta-9 desaturase activity, the concentration of 20:3(n-9), and triglyceride accumulation. This lipid metabolism disorder was associated with NADH accumulation due to mitochondrial dysfunction, and was reversed by the addition of pyruvate through NADH utilization.

Conclusions: The fatty acid enzyme, delta-9 desaturase, was activated by HCV core protein and polyunsaturated fatty acids counteracted this impact of the core protein on lipid metabolism. These results may open up new insights into the mechanism of lipid metabolism disorder associated with HCV infection and provide clues for the development of new therapeutic devices.

Keywords: Steatosis; Oleic acid; Core protein; Lipid metabolism; Desaturase; Hepatocellular carcinoma; NADH.

Received 31 March 2010; received in revised form 8 June 2010; accepted 5 July 2010; available online 22 September 2010

* Corresponding author. Address: Department of Gastroenterology, Graduate School of Medicine, University of Tokyo, 7-3-1 Hongo, Bunkyo-ku, Tokyo 113-8655, Japan. Tel.: +81 3 5800 8800; fax: +81 3 5800 8799.

E-mail address: kkoike-tky@umin.ac.jp (K. Koike).

Abbreviations: HCV, hepatitis C virus; HCC, hepatocellular carcinoma; PUFA, polyunsaturated fatty acids; PPAR, peroxisome proliferators-activated receptors; SREBP, sterol regulatory element binding protein; EPA, eicosapentaenoic acid; AA, arachidonic acid; ETYA, eicosatetraynoic acid; NADH, nicotinamide adenine dinucleotide; KBR, ketone body ratio.

Introduction

Persistent hepatitis C virus (HCV) infection leads to the development of chronic hepatitis, cirrhosis, and eventually, hepatocellular carcinoma (HCC), thereby being a serious problem worldwide both in medical and in socio-economical settings [1]. Histologically, several distinct features, such as bile duct damage, lymphoid follicle formation, and steatosis, (fatty change) characterize chronic hepatitis C [2–4]. Among these, steatosis is reproducible in experimental systems, both *in vitro* and *in vivo*, in which HCV proteins, particularly the core protein of HCV, are expressed. The introduced core gene induces the formation of lipid droplets in the cytoplasm of cultured cells [5,6], and in transgenic mice, it induces hepatic steatosis resembling that in chronic hepatitis C patients [7–10].

In addition, evidence has accumulated showing that steatosis is a crucial determining factor for the progression of liver fibrosis [11–13]. Steatosis and serum lipid profiles are also associated with sustained virological response to ribavirin/interferon combination therapy [14,15]. Moreover, HCV transgenic mice resemble chronic hepatitis C patients in terms of the development of HCC, implying that the HCV core protein is one of the most important viral molecules in the pathogenesis of hepatitis C [16,17]. It would thus be meaningful to explore the precise role of the core protein in modulating lipid metabolism, which may also be involved in hepatocarcinogenesis. More recently, involvement of the metabolism of lipids such as sphingolipids or cholesterol has been implicated in the replication of HCV, with a formation of lipid rafts, which are considered to be the place for HCV replication [18,19], hereby highlighting again the importance of lipid metabolism in HCV infection.

ELSEVIER

Journal of Hepatology **2011** vol. 54 | 432–438

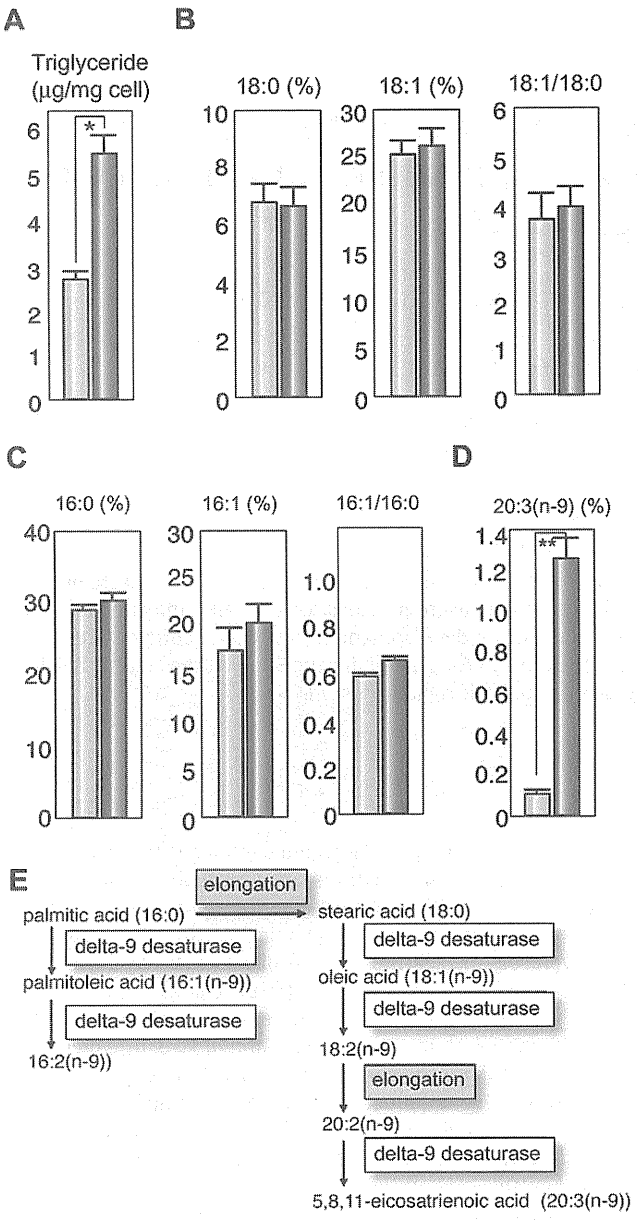

Fig. 1. Effect of the core protein on fatty acid composition in HepG2 cells. The fatty acid compositions of the total cell lipids were analyzed and the ratios of 18:1/18:0 and 16:1/16:0 in the core-expressing and control HepG2 cells were calculated. (A) Concentrations of triglycerides. (B) Percentages of stearic acid (18:0) and oleic acid (18:1(n-9)), and the 18:1/18:0 ratio. (C) Percentages of palmitic acid (16:0) and palmitoleic acid (16:1(n-9)), and the 16:1/16:0 ratio. (D) Percentage of eicosatrienoic acid (20:3(n-9)). (E) Schematic display of synthetic pathway of n-9 fatty acids. Light blue bars indicate control cells and dark blue bars indicate core-expressing cells. Values represent the mean ± SE, $n = 5$ in each group. $^{*}p < 0.05$, $^{**}p < 0.01$.

Previously, we reported that the concentration of oleic acid (18:1(n-9)) was increased compared with that of stearic acid (18:0) in liver tissues of chronic hepatitis C patients as well as in those of mice transgenic for the HCV core gene [8]. Such a change may lead to increased membrane fluidity, owing to the lower melting temperature of monounsaturated fatty acids, resulting in incremental metabolism and proliferation of hepatocytes [20–22]. On the other hand, polyunsaturated fatty acids (PUFAs), such as eicosapentaenoic acid (20:5(n-3)) and arachidonic acid (20:4(n-6)), are known to activate the nuclear transcription of peroxisome proliferator-activated receptors (PPAR) and suppress the sterol regulatory element binding protein (SREBP)-1. While PPARγ induces delta-9 desaturase (stearoyl-CoA desaturase) gene expression, PUFAs suppresses delta-9 desaturase activity [23]. In the current study, we determined fatty acid desaturase activities by analyzing the fatty acid compositions in HepG2 cells expressing HCV core protein by chromatography. In addition, we determined whether exogenous PUFAs restore HCV-associated changes in fatty acid metabolism.

Materials and methods

Reagents

Eicosapentaenoic acid (EPA), arachidonic acid (AA), and eicosatetraynoic acid (ETYA) were purchased from Sigma Chemical (St. Louis, MO). Other chemicals were of analytical grade and purchased from Wako Chemicals (Tokyo, Japan).

Cell culture

This study was performed using HepG2 cell lines expressing the HCV core protein under the control of the CAG promoter (Hep39J, Hep396 and Hep397), or a control HepG2 line (Hepswx) carrying an empty vector, which were described previously [24], and control bulk HepG2 cells. They were maintained in Dulbecco's modified Eagle's medium (DMEM), supplemented with 10% fetal bovine serum (Invitrogen), 1 mg/ml G418, 100 U/ml penicillin, and 100 μg/ml streptomycin in a humidified atmosphere at 37 °C in 5% CO_2. Fatty acids were dissolved in DMEM containing defatted bovine serum albumin. The ratio of fatty acids to albumin (mole/mole) was 0.7. The cells were exposed to fatty acid–albumin complexes at various concentrations for 48 h. All the experiments were repeated at least five times.

Lipid extraction, measurement of triglyceride content, and analysis of fatty acid composition

Total cell lipids were extracted by Foch's method. The cells were washed twice with phosphate-buffered saline and collected by centrifugation. The cell pellets were homogenized with 10 vole of chloroform: methanol solution (2:1), and the mixture was shaken for 5 min. The lower phase was then washed with 4 vole of saline, dried on anhydrous sodium sulfate, and evaporated to complete dryness. For the analysis of fatty acid composition, the residue was methanolysed by the modified Morrison and Smith method with boron trifluoride as a catalyst [25]. Fatty acid methyl esters were analyzed using a Shimadzu GC-7A gas chromatograph (Shimadzu Corp., Kyoto, Japan).

Measurement of the ketone body ratio and lactate/pyruvate

The cells were cultured to confluence on 3.5 cm dishes, and the medium was replaced with 700 μl of fresh one. After 24 h of incubation, the levels of acetoacetate and β-hydroxybutyrate in the medium were measured by monitoring the production or consumption of nicotinamide adenine dinucleotide (NADH) with Ketorex kit (Sanwa Chemical, Nagoya, Japan) [26]. The ketone body ratio (KBR) was calculated as the acetoacetate/β-hydroxybutyrate ratio. The lactate and pyruvate levels in the medium were measured at random times by the lactate oxidase method and pyruvate oxidase method, respectively.

Effect of pyruvate on lipid metabolism

In some experiments, pyruvate (Wako Chemicals) was added to culture medium at a final concentration of 0, 1, 5, or 10 mM. After 48 h of incubation at 37 °C, the cells were harvested and subjected to fatty acid composition analysis or real-time PCR analysis.

Real-time PCR

RNA was prepared from cultured cells using TRIzol LS (Invitrogen, Carlsbad, CA). The fluorescent signal was measured using ABI prism 7000 (Applied Biosystems, Tokyo, Japan). The genes encoding mouse sterol regulatory element-binding proteins (SREBP)-1a, SREBP-1c, delta-9 desaturase, and hypoxanthine phosphoribosyltransferase were amplified with the primer pairs CACAGCGGTTTTGAACGAC and CTGGCTCCTCTTTGATCCCA, ACGGAGCCATGGATTGCACATTTG and TACATCTT TAAAGCAGCGGGTGCCGATGGT, TTCCCTCCTGCAAGCTCTAC and CGCAAGAAGG TGCTAACGAAC, and CCAGCAAGCTTGCAACCTTAACCA and GTAATGATCAGTCAAC GGGGGAC, respectively.

Statistical analysis

Data are presented as the mean ± SE. The data were analyzed by Mann–Whitney *U* test. Differences were considered statistically significant when $p < 0.05$.

Results

Triglyceride content in HepG2 cells expressing HCV core protein

To validate the relationship between the lipid accumulation and the core protein, we first determined the triglyceride contents in core-protein-expressing HepG2 clones (core-expressing cells), Hep39J, Hep396, Hep397, and control HepG2 cells. Core-expressing Hep396 cells contained significantly larger amounts of triglyceride than the control cells (Fig. 1A, $p < 0.01$), which are consistent with the results of previous studies on culture cells and transgenic mice [6,7,27]. Similar results were obtained with the other core-expressing cell lines.

Fatty acid compositions of total cell lipids

Analysis on the fatty acid compositions of total lipids revealed that the concentration of oleic acid (18:1(n-9)) and the ratio of oleic acid/stearic acid (18:1/18:0) in the core-expressing cells are similar to those in the control cells (Fig. 1B). The ratio of palmitoleic acid (16:1(n-9))/palmitic acid (16:1/16:0) was higher in the core-expressing cells than that in the control cells, but the difference was not significant (Fig. 1C). This rather dissociates from the results obtained in HCV core gene transgenic mice, in which the 18:1/18:0 ratio was significantly higher than that in control mice, thereby suggesting an increased delta-9 desaturase activity as a consequence of the HCV core protein expression [8]. However, it should be noted that the concentration of 5,8,11-eicosatrienoic acid (20:3(n-9)), a downstream product of n-9 fatty acid desaturation, was approximately13 times higher in the core-expressing cells than that in the control cells (Fig. 1D and E, $p < 0.01$). This is due to the fact that the activity of the delta-6 desaturase, an enzyme downstream of delta-9 desaturase, is also high in HepG2 cells, resulting in the relatively lower concentration of 18:1 in the core-expressing cells despite the high delta-9 desaturase activity. Actually, the delta-6 desaturase activity has been shown to be inherently high in HepG2 cells [28,29].

To verify this possibility, we administered ETYA, which inhibits delta-6 desaturase activity, to the cell cultures. Because similar results were obtained with the other core-expressing HepG2 cell lines, subsequent experiments were carried out using the Hep396 cell line. The addition caused significant increases in both 18:1/18:0 and 16:1/16:0 ratios in the core-expressing cells but not in the control cells (Fig. 2A 0 vs. 10 μg/ml and 0 vs. 50 μg/ml; $p < 0.05$, respectively). When compared between the

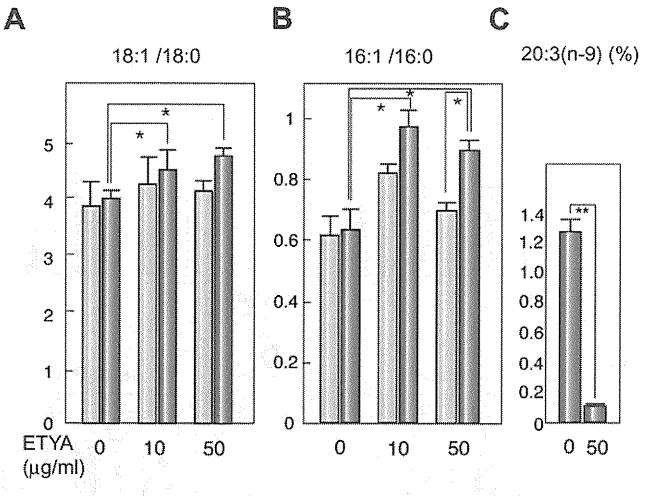

Fig. 2. Effect of ETYA on delta-9 desaturase index. HepG2 cells with or without the core protein were incubated with ETYA for 48 h. The fatty acid compositions of the total cell lipids were analyzed, and the ratios of 18:1/18:0 (A) and 16:1/16:0 (B), and the percentage of eicosatrienoic acid (20:3(n-9) (C) were computed. Light blue bars indicate control cells and dark blue bars indicate core-expressing cells. $N = 5$ in each group. *$p < 0.05$. ETYA, eicosatetraynoic acid.

core-expressing cells and control cells after the treatment with 50 μg/ml ETYA, the 18:1/18:0 ratio was higher and the 16:1/16:0 ratio was significantly higher (Fig. 2B, $p < 0.05$) in the core-expressing cells. ETYA (50 μg/ml) significantly decreased the concentration of 20:3(n-9) in the core-expressing cells (Fig. 2C, $p < 0.01$). These results suggest that the HCV core protein enhances the activities of delta-9, and possibly, delta-5 desaturases, modulating fatty acid metabolism in HepG2 cells, in which the delta-6 desaturase activity is intrinsically high (Fig. 1E) [28,29].

PUFAs modify fatty acid compositions and decrease triglyceride contents in HepG2 Cells

PUFAs are known to suppress the activities of both delta-9 and delta-6 desaturases. We, therefore, added PUFA, EPA, or AA, to the culture cell medium to examine the effect of PUFAs on the fatty acid compositions in HepG2 cells expressing the core protein. EPA and AA individually decreased the 18:1/18:0 and 16:1/16:0 ratios in a similar extent in both the core-expressing cells and the control cells (Fig. 3, $p < 0.05$). EPA and AA also significantly decreased the concentration of 20:3(n-9) in the core-expressing cells in a dose-dependent manner (Fig. 4, $p < 0.05$). In addition, EPA and AA individually decreased the triglyceride concentration in cells, in particular, in the core-expressing cells (Fig. 5, in core-expressing cells, $p < 0.01$; in control cells, $p < 0.05$, respectively).

Ketone body ratio and lactate/pyruvate ratio

Although the mechanism by which the HCV core protein enhances fatty acid desaturation is yet unclear, one possibility is the creation of an overreduced state in the core-expressing cells. The overreduced state or the accumulation of NADH in cells is known to accelerate the activities of fatty acid desaturases [30,31]. Such a condition may originate from the dysfunction of the mitochondrial electron transfer system (ETS), which has been

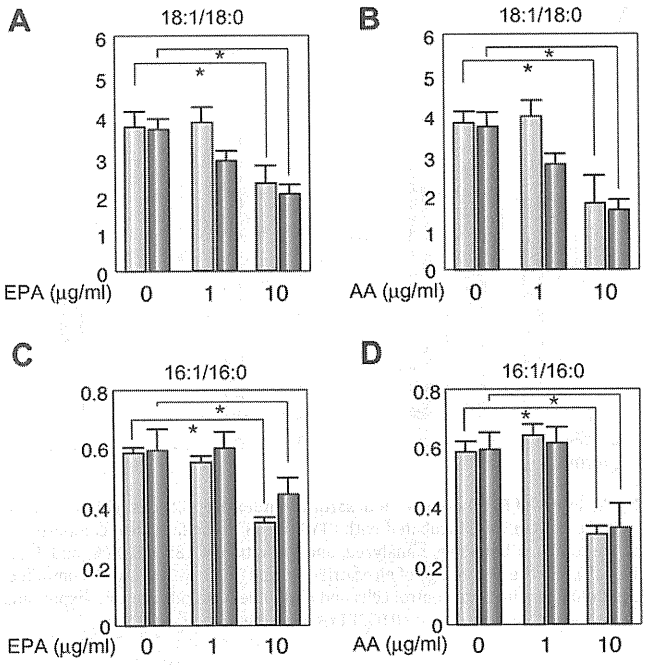

Fig. 3. Effect of EPA and AA on delta-9 desaturase index. HepG2 cells with or without the core protein were incubated with EPA (A and C) or AA (B and D) for 48 h. The fatty acid compositions of the total cell lipids were analyzed and the ratios of 18:1/18:0 (A and B) and 16:1/16:0 (C and D) were computed. Light blue bars indicate control cells and dark blue bars indicate core-expressing cells. $N = 5$ in each group. $^{*}p < 0.05$. EPA, eicosapentaenoic acid; AA, arachidonic acid.

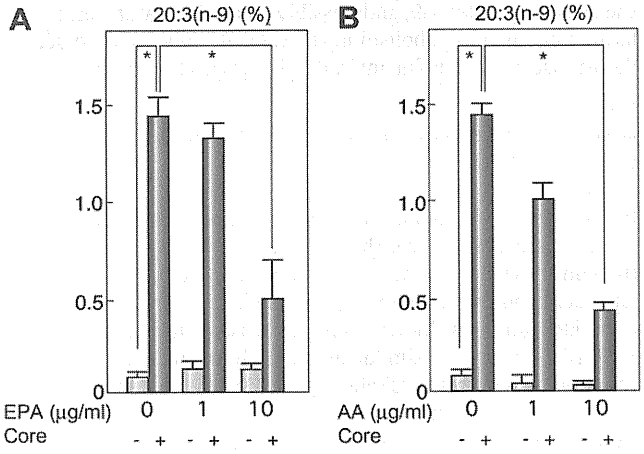

Fig. 4. Effect of EPA and AA on the concentration of 20:3(n-9). HepG2 cells with or without the core protein were incubated with EPA (A) or AA (B) for 48 h. The fatty acid compositions of the total cell lipids were analyzed and the percentages of the C20:3(n-9) fraction were measured. Light blue bars indicate control cells and dark blue bars indicate core-expressing cells. $N = 5$ in each group. $^{*}p < 0.05$.

suggested to be associated with HCV infection by the action of the HCV core protein [32–35]. Then, we explored the possibility that an increase in the NADH level, which is caused by the mitochondrial ETS dysfunction, induces the activation of fatty acid desaturases. Because fatty acid synthesis or fatty acid desaturation is accompanied by the oxidation of NAD(P)H, we measured the ketone body ratio (KBR) in the culture medium to estimate the redox state in the HepG2 cells expressing the core protein.

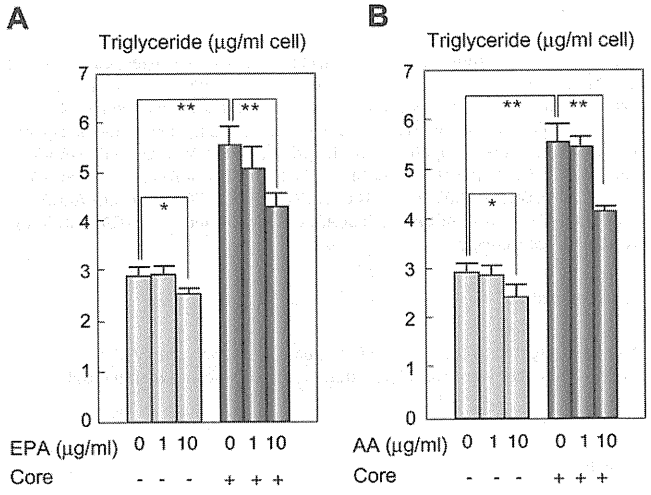

Fig. 5. Effect of EPA and AA on triglyceride content. HepG2 cells with or without the core protein were incubated with EPA (A) or AA (B) for 48 h. The triglyceride volume of the total cell lipids was measured and the triglyceride contents in the cells were calculated. Light blue bars indicate control cells and dark blue bars indicate core-expressing cells. $N = 5$ in each group. $^{*}p < 0.05$, $^{**}p < 0.01$.

The KBR, which is in equilibrium with the intramitochondrial $NAD^+/NADH$ [26,36], in the culture medium of the core-expressing cells, was significantly lower than that of control cells (Fig. 6A, $p < 0.01$). The ratio of lactate to pyruvate (lactate/pyruvate), which is proportional to the cytosolic $NADH/NAD^+$ [26], in the culture medium of the core-expressing cells was significantly higher than that of control cells (Fig. 6B, $p < 0.05$). These results, the higher $NADH/NAD^+$ ratio in both determinations, indicate that NADH accumulates in the core-expressing HepG2 cells, resulting in the overreduced state, as a consequence of the core protein expression. The amounts of total ketone bodies were significantly higher in the core-expressing cells than that in the control cells (Fig. 6C).

Effects of pyruvate on lipid metabolism in core-expressing cells

The addition of pyruvate into this constitutive core protein expression system, in which the pyruvate metabolism is in equilibrium, is expected to cause a reduction in the NADH level along with increases in the levels of lactate and NAD^+, because pyruvate tends to be converted to lactate by the action of lactate dehydrogenase (LDH) under the condition of high $NADH/NAD^+$ ratio [26,36]. Actually, the addition of pyruvate into the culture medium at various concentrations increased the KBR and reduced the amount of 5,8,11-eicosatrienoic acid (20:3 (n-9)) (Fig. 6D, $p < 0.05$ at 10 mM pyruvate), while it had no effect on the control cells. It also caused a reduction in the amount of triglyceride in the core-expressing cells but not in the control cells (Fig. 6E). This finding strongly supports the notion that NADH accumulation is, at least, one of the causes of the activation of fatty acid desaturases in this HCV model. The mRNA levels of anti-oxidant genes significantly decreased after the incubation with pyruvate at 10 mM (catalase, 1.27 ± 0.06 vs. 0.91 ± 0.05; glutathione synthetase 1.39 ± 0.04 vs. 1.01 ± 0.06; glutathione peroxidase 1.48 ± 0.03 vs. 1.23 ± 0.07, pyruvate (−) vs. pyruvate (+), $p < 0.05$, respectively), suggesting that pyruvate reduced the levels of oxidative stress in the core-expressing HepG2 cells.

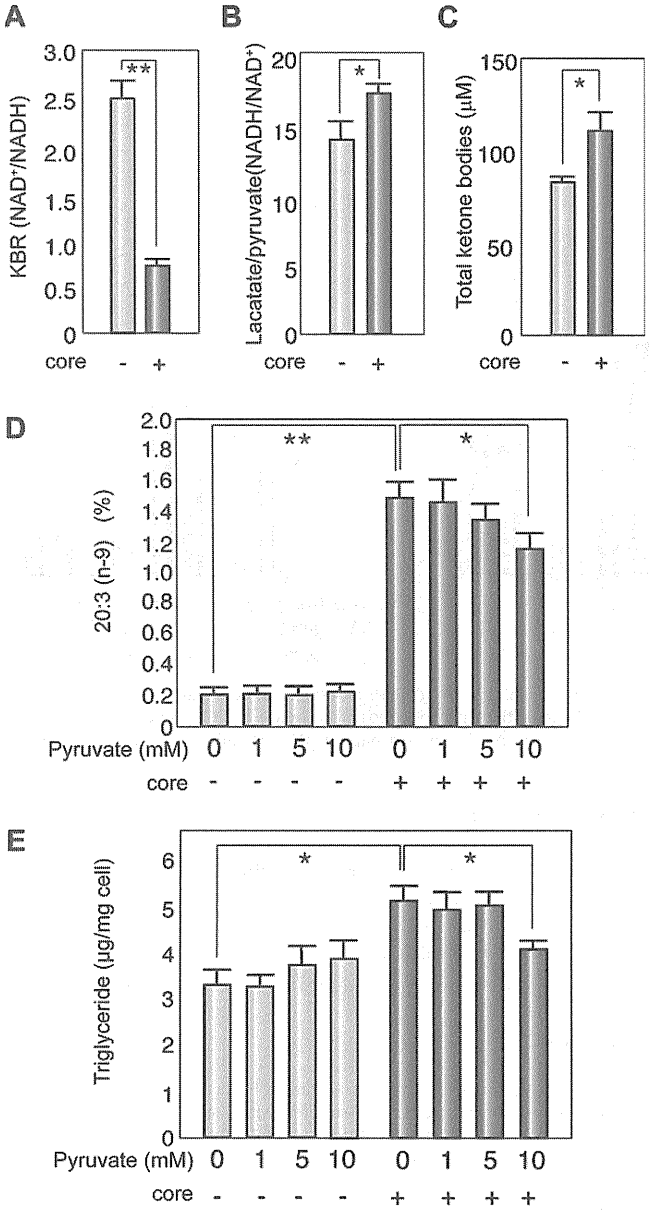

Fig. 6. NADH accumulation and effect of pyruvate in core-expressing cells. HepG2 cells with or without the core protein were subjected to the determination of ketone body ratio (A) and lactate/pyruvate ratio (B) for the precise estimation of NAD^+/NADH and NADH/NAD^+. (C) Total ketone bodies. (D) The percentages of the C20:3(n-9) fraction were measured after incubation with pyruvate at various concentrations. (E) The total amount of triglyceride was measured after incubation with pyruvate at various concentrations. Light blue bars indicate control cells and dark blue bars indicate core-expressing cells. $N = 5$ in each group. $^*p < 0.05$, $^{**}p < 0.01$.

Expression of SREBP-1 and desaturase genes in core-expressing cells

We previously showed that the core protein activates the expression of the SREBP-1c gene, which regulates the production of triglyceride [37] in the liver. We, therefore, examined the mRNA levels of genes associated with lipid metabolism in the current system. As shown in Fig. 7, the mRNA levels of SREBP-1c and delta-9 (stearoyl CoA) desaturase genes, but not that of the SREBP-1a gene, were significantly higher in the core-expressing cells than that in the control cells. Of note, the mRNA levels of the former two genes significantly decreased after the incubation with AA. The treatment with pyruvate also reduced the mRNA levels of the two genes, but the difference was not statistically significant compared with the control.

Discussion

The core protein of HCV modulated the activities of delta desaturases and changed the saturation states of fatty acids. The observed change in the HepG2 cells, namely, an increase in the amounts of unsaturated fatty acids, may support cell proliferation, by increasing the fluidity of the cell membrane as reported previously [20]. In the HepG2 cells expressing the core protein, the delta-6 desaturase activity was as high as that of the delta-9 desaturase, leading to the accumulation of a downstream product, 20:3(n-9) fatty acid. This was, unexpectedly, in contrast to our previous result on the liver tissues of HCV core gene transgenic mice, in which the 18:1/18:0 and 16:1/16:0 ratios were significantly higher than that in the liver tissues of normal littermate mice, indicating the activation of delta-9 desaturase [8]. The 16:1/16:0 and 18:1/18:0 ratios observed in the control HepG2 cells were consistent with the results of a previous study: the delta-6 desaturase activity is inherently higher in HepG2 cells than in normal mouse hepatocytes [28,29]. This may explain the difference in the effect of the core protein on lipid metabolism in these two systems, namely, HepG2 cells and mouse liver tissues. The significant increase in the delta-9 desaturase index and high concentration of 20:3(n-9) by the administration of ETYA, a delta-6 desaturase inhibitor, indicate the activation of delta-9 desaturase in the core-expressing cells. The results of real-time PCR analysis for determining the mRNA levels of these enzymes corroborated the current estimation of desaturase activities as determined by fatty acid analysis.

The mechanism underlying the activation of fatty acid desaturation by the HCV core protein is still unclear, but one possibility is the presence of an overreduced state in the core-expressing cells. The HCV core protein is closely associated with mitochondrial dysfunction, in particular, that of the respiratory chain complexes, resulting in an impairment of NADH oxidation [32–35]. NADH accumulation leads to an increase in desaturase activities through the augmentation of microsomal electron transfer [38]. In fact, the KBR in the core-expressing cells was significantly lower than that in the control cells, indicating the accumulation of NADH within the cells. The addition of pyruvate resulted in an increase in the KBR and a reduction in the amounts of triglyceride and 5,8,11-eicosatrienoic acid (20:3 (n-9)) while it had no effect on the control cells, strongly supporting the notion that NADH accumulation induced by the core protein is, at least, one of the causes of the activation of fatty acid desaturases in this HCV model.

Another possible mechanism underlying the accelerated desaturation is the activation of SREBP-1c, which controls the expression of delta-9 desaturase. In fact, the level of SREBP-1c mRNA was higher in the core-expressing cells than that in the control cells as reported previously [37]. The relief of NADH accumulation by pyruvate administration resulted in the reduced accumulation of triglyceride and unsaturated fatty acids, which was accompanied by the reduction in SREBP-1c and delta-9 desaturase gene expression levels. The intracellular accumulation of NADH might be involved in the activation of the SREBP-1c gene expression by the core protein. Thus, NADH accumulation, which

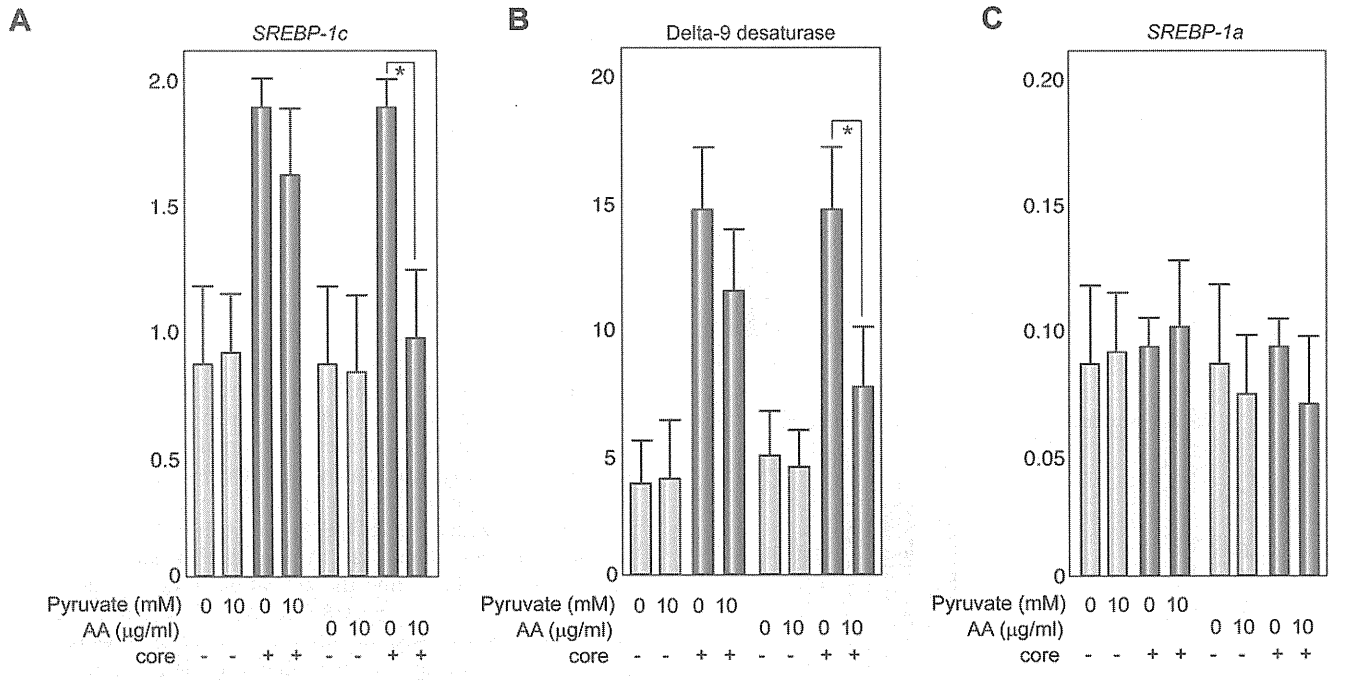

Fig. 7. Effect of pyruvate and AA on mRNA levels of lipid-associated genes. The mRNA levels of *SREBP-1c* (A), delta-9 desaturase (B) and *SREBP-1a* (C) genes were determined by real-time PCR analysis. The transcription of the genes was normalized with that of hypoxanthine phosphoribosyltransferase, and the values are expressed as relative activities. Light blue bars indicate control cells and dark blue bars indicate core-expressing cells. $N = 5$ in each group. $^{*}p < 0.05$. SREBP, sterol regulatory element binding protein.

is induced by the core protein through the impairment of the mitochondrial complex function [35], may be a key event that leads to the SREBP-1c activation, the desaturase activation, and the development of steatosis associated with HCV infection.

EPA and AA (PUFAs), which are known to suppress desaturase activities, lowered the 18:1/18:0 and 16:1/16:0 ratios and decreased the concentration of 20:3(n-9) concomitantly with that of triglyceride, regardless of the presence of the core protein, probably through SREBP-1c suppression (Fig. 7) [39]. On the other hand, the administration of EPA or AA did not affect the KBR in the core-expressing or control cells (data not shown), limiting the PUFAs ability to counteract the effect of the core protein. This is in contrast to the fact that the addition of pyruvate caused an increase in the KBR and a reduction in the amounts of triglyceride and 5,8,11-eicosatrienoic acid (20:3 (n-9)), while it had no effect on the control cells.

Fatty acid desaturation is closely associated with increased membrane fluidity [20], leading to augmented cell metabolism and higher cell division rates [21,22]. Although the relationship between carcinogenesis and lipid metabolism altered by the HCV core protein remains to be further clarified, alterations in lipid metabolism, in particular, in the desaturation of fatty acids, are closely associated with HCV infection, and PUFAs could prevent the pathogenesis of HCV-associated disorders involving lipid metabolism.

Conflict of interest

The authors who have taken part in this study declared that they do not have anything to disclose regarding funding or conflict of interest with respect to this manuscript.

Acknowledgments

This work was supported in part by Grant-in-Aid for Scientific Research on Priority Area from the Ministry of Education, Science, Sports, and Culture of Japan; Health Sciences Research Grants of The Ministry of Health, Labour, and Welfare (Research on Hepatitis); and a grant from The Sankyo Foundation of Life Science.

References

[1] Saito I, Miyamura T, Ohbayashi A, Harada H, Katayama T, Kikuchi S, et al. Hepatitis C virus infection is associated with the development of hepatocellular carcinoma. Proc Natl Acad Sci USA 1990;87:6547–6549.
[2] Schemer PJ, Ashrafzadeh P, Sherlock S, Brown D, Dusheiko GM. The pathology of chronic hepatitis C. Hepatology 1992;15:567–571.
[3] Bach N, Thung SN, Schaffner F. The histological features of chronic hepatitis C and autoimmune chronic hepatitis: a comparative analysis. Hepatology 1992;15:572–577.
[4] Fujie H, Yotsuyanagi H, Moriya K, Shintani Y, Tsutsumi T, Takayama T, et al. Steatosis and intrahepatic hepatitis C virus in chronic hepatitis. J Med Virol 1999;59:141–145.
[5] Moradpour D, Englert C, Wakita T, Wands JR. Characterization of cell lines allowing tightly regulated expression of hepatitis C virus core protein. Virology 1996;222:51–63.
[6] Barba G, Harper F, Harada T, Kohara M, Goulinet S, Matsuura Y, et al. Hepatitis C virus core protein shows a cytoplasmic localization and associates to cellular lipid storage droplets. Proc Natl Acad Sci USA 1997;94:1200–1205.
[7] Moriya K, Yotsuyanagi H, Shintani Y, Fujie H, Ishibashi K, Matsuura Y, et al. Hepatitis C virus core protein induces hepatic steatosis in transgenic mice. J Gen Virol 1997;78:1527–1531.
[8] Moriya K, Todoroki T, Tsutsumi T, Fujie H, Shintani Y, Miyoshi H, et al. Increase in the concentration of carbon 18 monosaturated fatty acids in the liver with hepatitis C: analysis in transgenic mice and humans. Biophys Biochem Res Commun 2001;281:1207–1212.
[9] Lerat H, Honda M, Beard MR, Loesch K, Sun J, Yang Y, et al. Steatosis and liver cancer in transgenic mice expressing the structural and nonstructural proteins of hepatitis C virus. Gastroenterology 2002;122:352–365.

[10] Naas T, Ghorbani M, Alvarez-Maya I, Lapner M, Kothary R, De Repentigny Y, et al. Characterization of liver histopathology in a transgenic mouse model expressing genotype 1a hepatitis C virus core and envelope proteins 1 and 2. J Gen Virol 2005;86:2185–2196.
[11] Adinolfi LE, Gambardella M, Andreana A, Tripodi MF, Utili R, Ruggiero G. Steatosis accelerates the progression of liver damage of chronic hepatitis C patients and correlates with specific HCV genotype and visceral obesity. Hepatology 2001;33:1358–1364.
[12] Massard J, Ratziu V, Thabut D, Moussalli J, Lebray P, Benhamou Y, et al. Natural history and predictors of disease severity in chronic hepatitis C. J Hepatol 2006;44:S19–S24.
[13] Leandro G, Mangia A, Hui J, Fabris P, Rubbia-Brandt L, Colloredo G, et al. HCV meta-analysis (on) individual patients' data study group. Relationship between steatosis, inflammation, and fibrosis in chronic hepatitis C: a meta-analysis of individual patient data. Gastroenterology 2006;130:1636–1642.
[14] Patton HM, Patel K, Behling C, Bylund D, Blatt LM, Vallee M, et al. The impact of steatosis on disease progression and early and sustained treatment response in chronic hepatitis C patients. J Hepatol 2004;40: 484–490.
[15] Harrison SA, Brunt EM, Qazi RA, Oliver DA, Neuschwander-Tetri BA, Di Bisceglie AM, et al. Effect of significant histologic steatosis or steatohepatitis on response to antiviral therapy in patients with chronic hepatitis C. Clin Gastroenterol Hepatol 2005;3:604–609.
[16] Moriya K, Fujie H, Shintani Y, Yotsuyanagi H, Tsutsumi T, Ishibashi K, et al. The core protein of hepatitis C virus induces hepatocellular carcinoma in transgenic mice. Nat Med 1998;4:1065–1067.
[17] Koike K. Molecular basis of hepatitis C virus-associated hepatocarcinogenesis: lessons from animal model studies. Clin Gastroenterol Hepatol 2005;3:S132–S135.
[18] Shi ST, Lee KJ, Aizaki H, Hwang SB, Lai MM. Hepatitis C virus RNA replication occurs on a detergent-resistant membrane that cofractionates with caveolin-2. J Virol 2003;77:4160–4168.
[19] Miyanari Y, Atsuzawa K, Usuda N, Watashi K, Hishiki T, Zayas M, et al. The lipid droplet is an important organelle for hepatitis C virus production. Nat Cell Biol 2007;9:1089–1097.
[20] Stubbs CD, Smith AD. The modification of mammalian membrane polyunsaturated fatty acid composition in relation to membrane fluidity and function. Biochim Biophys Acta 1984;779:89–137.
[21] Li J, Ding SF, Habib NA, Fermor BF, Wood CB, Gilmour RS. Partial characterization of a cDNA for human stearoyl-CoA desaturase and changes in its mRNA expression in some normal and malignant tissues. Int J Cancer 1994;57:348–352.
[22] Vinciguerra M, Carrozzino F, Peyrou M, Carlone S, Montesano R, Benelli R, et al. Unsaturated fatty acids promote hepatoma proliferation and progression through downregulation of the tumor suppressor PTEN. J Hepatol 2009;50:1132–1141.
[23] Ntambi JM. Regulation of stearoyl-CoA desaturase by polyunsaturated fatty acids and cholesterol. J Lipid Res 1999;40:1549–1558.
[24] Ruggieri A, Murdolo M, Harada T, Miyamura T, Rapicetta M. Cell cycle perturbation in a human hepatoblastoma cell line constitutively expressing hepatitis C virus core protein. Arch Virol 2004;149:61–74.
[25] Morrison WR, Smith LM. Preparation of fatty acid methyl esters and dimethylacetals from lipids with boron fluoride–methanol. J Lipid Res 1964;5:600–608.
[26] Williamson DH, Mellanby J, Krebs HA. Enzymic determination of D(-)-beta-hydroxybutyric acid and acetoacetic acid in blood. Biochem J 1962;82:90–96.
[27] Abid K, Pazienza V, Gottardi A, Rubbia-Brandt L, Conne B, Pugnale P, et al. An in vitro model of hepatitis C virus genotype 3a-associated triglycerides accumulation. J Hepatol 2005;42:744–751.
[28] Portolesi R, Powell BC, Gibson RA. Delta6 desaturase mRNA abundance in HepG2 cells is suppressed by unsaturated fatty acids. Lipids 2008;43:91–95.
[29] Choi Y, Park Y, Pariza MW, Ntambi JM. Regulation of stearoyl-CoA desaturase activity by the trans-10, cis-12 isomer of conjugated linoleic acid in HepG2 cells. Biochem Biophys Res Commun 2001;284:689–693.
[30] Strittmatter P, Spatz L, Corcoran D, Rogers MJ, Setlow B, Redline R. Purification and properties of rat liver microsomal stearyl coenzyme a desaturase. Proc Natl Acad Sci USA 1974;71:4565–4569.
[31] Joshi VC, Wilson AC, Wakil SJ. Assay for the terminal enzyme of the stearoyl coenzyme A desaturase system using chick embryo liver microsomes. J Lipid Res 1977;18:32–36.
[32] Korenaga M, Wang T, Li Y, Showalter LA, Chan T, Sun J, et al. Hepatitis C virus core protein inhibits mitochondrial electron transport and increases reactive oxygen species (ROS) production. J Biol Chem 2005;280: 37481–37488.
[33] Piccoli C, Scrima R, Quarato G, D'Aprile A, Ripoli M, Lecce L, et al. Hepatitis C virus protein expression causes calcium-mediated mitochondrial bioenergetic dysfunction and nitro-oxidative stress. Hepatology 2007;46:58–65.
[34] Tsutsumi T, Matsuda M, Aizaki H, Moriya K, Miyoshi H, Fujie H, et al. Proteomics analysis of mitochondrial proteins reveals overexpression of a mitochondrial protein chaperone, prohibitin, in cells expressing hepatitis C virus core protein. Hepatology 2009;50:378–386.
[35] Moriya K, Miyoshi H, Tsutsumi T, Shinzawa S, Fujie H, Shintani Y, et al. Tacrolimus ameliorates metabolic disturbance and oxidative stress caused by hepatitis C virus core protein: Analysis using mouse model and cultured cells. Am J Pathol 2009;175:1515–1524.
[36] Williamson DH, Lund P, Krebs HA. The redox state of free nicotinamide-adenine dinucleotide in the cytoplasm and mitochondria of rat liver. Biochem J 1967;103:514–527.
[37] Moriishi K, Mochizuki R, Moriya K, Miyamoto H, Mori Y, Abe T, et al. Critical role of PA28gamma in hepatitis C virus-associated steatogenesis and hepatocarcinogenesis. Proc Natl Acad Sci USA 2007;104:1661–1666.
[38] Jansson I, Schenkman JB. Studies on three microsomal electron transfer enzyme systems. Specificity of electron flow pathways. Arch Biochem Biophys 1977;178:89–107.
[39] Sekiya M, Yahagi N, Matsuzaka T, Najima Y, Nakakuki M, Nagai R, et al. Polyunsaturated fatty acids ameliorate hepatic steatosis in obese mice by SREBP-1 suppression. Hepatology 2003;38:1529–1539.

Oncology

Oncology 2011;81(suppl 1):11–17
DOI: 10.1159/000333253

Published online: December 22, 2011

Hepatocarcinogenesis in Hepatitis C: HCV Shrewdly Exacerbates Oxidative Stress by Modulating both Production and Scavenging of Reactive Oxygen Species

Hidetake Fujinaga Takeya Tsutsumi Hiroshi Yotsuyanagi Kyoji Moriya
Kazuhiko Koike

Department of Internal Medicine, Graduate School of Medicine, The University of Tokyo, Tokyo, Japan

Key Words
Hepatitis C · Hepatocellular carcinoma · Oxidative stress · Transgenic mouse · Core protein

Abstract
Persistent infection with hepatitis C virus (HCV) is a major risk for the development of hepatocellular carcinoma (HCC). One of the characteristics of HCV infection is the unusual augmentation of oxidative stress, which is exacerbated by iron accumulation in the liver, as observed frequently in hepatitis C patients. Using a transgenic mouse model, in which HCC develops late in life after the preneoplastic steatosis stage, the core protein of HCV was shown to induce the overproduction of reactive oxygen species (ROS) in the liver. In excessive generation of ROS, HCV affects the steady-state levels of a mitochondrial protein chaperone, i.e. prohibitin, leading to an impaired function of the mitochondrial respiratory chain with the overproduction of ROS. Insulin resistance and hepatic steatosis, which frequently accompany HCV infection, exacerbate ROS production. On the other hand, HCV compromises some of the antioxidant systems, including heme oxygenase-1 and NADH dehydrogenase quinone 1, resulting in the provocation of oxidative stress, together with ROS overproduction, in the liver with HCV infection. Thus, HCV infection not only induces ROS but also hampers the antioxidant system in the liver, thereby exacerbating oxidative stress that would facilitate hepatocarcinogenesis. Combination with the other activated pathway, including an alteration in the intracellular signaling cascade of MAP kinase, along with HCV-associated disturbances in lipid and glucose metabolism would lead to the unusual mode of hepatocarcinogenesis, i.e. very frequent and multicentric development of HCC, in persistent HCV infection.

Introduction

Approximately 200 million people are infected with hepatitis C virus (HCV) worldwide. More than two thirds of those with acute HCV infection suffer from persistent infection causing active or inactive chronic hepatitis, and approximately 30% of patients with chronic hepatitis are assumed to develop cirrhosis within their lifetime. Once HCV infection develops into cirrhosis, hepatocellular carcinoma (HCC) develops at an annual rate of 7% [1]. The strong association of oxidative stress with HCV infection has been demonstrated and can explain at least part of the clinical progression of the disease. The patho-

KARGER

Fax +41 61 306 12 34
E-Mail karger@karger.ch
www.karger.com

0030–2414/11/0817–0011$38.00/0

Accessible online at:
www.karger.com/ocl

Kazuhiko Koike, MD, PhD
Department of Gastroenterology, Graduate School of Medicine
The University of Tokyo
7-3-1 Hongo, Bunkyo-ku, Tokyo 113-8655 (Japan)
Tel. +81 3 5800 8800, E-Mail kkoike-tky@umin.ac.jp

genesis of chronic hepatitis C is not merely ascribed to inflammation caused by viral infection; the role of viral proteins in the pathogenesis has also been reported [2]. Of the proteins constituting HCV, the core protein in particular has various functions with respect to host cells and is closely related to oxidative stress. In this article, the relationship between HCV infection and oxidative stress is analyzed focusing on the pathological effect of the core protein of HCV, and the significance of oxidative stress in the pathogenesis of liver disease is discussed.

HCV Infection and Hepatocarcinogenesis

The mechanism underlying hepatocarcinogenesis in HCV infection is not fully understood yet. Inflammation induced by an immune response to HCV should be considered, of course, in a study on hepatocarcinogenesis in hepatitis viral infection: necrosis of hepatocytes due to chronic inflammation followed by regeneration enhances genetic aberrations in host cells, the accumulation of which culminates in HCC. This theory presupposes an indirect involvement of hepatitis viruses in HCC via hepatic inflammation. However, this context leaves us with a serious question: can inflammation alone result in the development of HCC in HCV infection with such a high incidence (90% in 15 years) or in a multicentric fashion? The other role of HCV would have to be weighed against a rare occurrence of HCC, even after the development of cirrhosis, in patients with autoimmune hepatitis in which severe inflammation in the liver persists. These backgrounds and reasonings lead to a possible activity of viral proteins for inducing neoplasia. This possibility has been evaluated by introducing genes of HCV into hepatocytes in culture with little success. One of the difficulties in using cultured cells is the carcinogenic capacity of HCV, if any, which would be weak and would take a long time to manifest itself. Actually, it takes 30–40 years for HCC to develop in individuals infected with HCV. On the basis of these viewpoints, we started to investigate carcinogenesis in chronic hepatitis C in vivo using transgenic mouse technology.

Transgenic Mouse Model for HCV-Related HCC

One of the major issues regarding the pathogenesis of HCV-associated liver lesions is whether the HCV proteins have direct effects on pathological phenotypes. For this purpose, several lines of mice have been established which are transgenic for the HCV cDNA. We have engineered transgenic mouse lines carrying the HCV genome by introducing the genes from the cDNA of the HCV genome of genotype 1b [3, 4]. Four different kinds of transgenic mouse lines are established, and they carry the core gene, envelope genes, the entire nonstructural (NS) genes, or the NS5A gene, respectively, under the same transcriptional regulatory element. Among these mouse lines, only the transgenic mice carrying the core gene developed HCC in two independent lineages [4]. The envelope gene transgenic mice did not develop HCC despite high expression levels of both E1 and E2 proteins [5], and the transgenic mice carrying the entire NS or NS5A gene developed no HCC.

Early in life, core gene transgenic mice develop hepatic steatosis, which is one of the histologic characteristics of chronic hepatitis C, along with lymphoid follicle formation and bile duct damages [6]. Thus, the core gene transgenic mouse model well reproduces the feature of chronic hepatitis C. It is important to note that no significant inflammation is observed in the liver of this animal model. Late in life, these transgenic mice develop HCC. Notably, the development of steatosis and HCC has been reproduced by other HCV transgenic mouse lines, which harbor the structural genes including the core gene [4, 7, 8]. These outcomes indicate that the core protein per se of HCV has an oncogenic potential when expressed in vivo.

Augmentation of Oxidative Stress in Hepatitis C

There is a notable feature in the localization of the core protein in hepatocytes; while the core protein predominantly exists in the cytoplasm associated with lipid droplets, it is also present in the mitochondria and nuclei [4]. On the basis of this finding, the pathways related to these two organelles, the mitochondria and nuclei, were thoroughly investigated.

One effect of the core protein is an increased production of oxidative stress in the liver. We would like to draw particular attention to the fact that the production of oxidative stress is increased in the core gene transgenic mouse model in the absence of inflammation in the liver [4]. The overproduction of oxidative stress results in the generation of deletions in the mitochondrial and nuclear DNA, an indicator of genetic damage [2].

Augmentation of oxidative stress is implicated in the pathogenesis of liver disease in HCV infection as shown by a number of clinical and basic studies [2, 9]. Reactive

oxygen species (ROS) are endogenous oxygen-containing molecules formed as normal products during aerobic metabolism. ROS can induce genetic mutations as well as chromosomal alterations and thus contribute to cancer development in multistep carcinogenesis [10, 11]. Recent studies have shown that oxidative stress is more augmented in hepatitis C than in other types of hepatitis such as hepatitis B [9].

Thus, a major role in the pathogenesis of HCV-associated liver disease has been attributed to oxidative stress augmentation, but little is known regarding the mechanism of increased oxidative stress in HCV infection. Hence, it is important to understand the mechanism of oxidative stress augmentation, in terms of both generation and scavenging of ROS, which may allow us to develop new tools of therapies for chronic hepatitis C.

Oxidative Stress and the Liver

Oxidative Stress and Reactive Oxygen

The main source of ROS in hepatocytes is the mitochondria. Outside of hepatocytes, ROS also originate from nicotinamide adenine dinucleotide phosphate (NADPH) oxidase and xanthine oxidase in Kupffer cells and inflammatory cells. A large percentage of consumed oxygen is constantly converted into ROS in the mitochondria accompanied by oxygen consumption in the electron transport system (ETS). Hepatocytes contain many mitochondria and therefore have a high ROS production. Generated ROS are very unstable and highly reactive and attack biomolecules such as DNA, lipids, and proteins. The liver not only produces much ROS but is also the center of the antioxidative effect in the form of protein synthesis. Oxidative stress refers to the oxidation-reaction-dominant state of the living body induced by an imbalance between the oxidation reaction caused by ROS and the antioxidation reaction. Main ROS include superoxide ($\cdot O_2^-$), hydrogen peroxide (H_2O_2), and the hydroxyl radical ($HO\cdot$). ROS are mainly produced from $\cdot O_2^-$ and converted into stable H_2O_2 through a dismutation reaction. H_2O_2 is converted into highly reactive $HO\cdot$ in the presence of a transition metal.

The Antioxidant System and Oxidative Stress Markers

Antioxidants include glutathione (GSH), thioredoxin (TRX), vitamin E, vitamin C, and β-carotene. Reactive oxygen elimination enzymes include superoxide dismutase (SOD), GSH peroxidase, heme oxygenase (HO)-1, and catalase. SOD is induced by oxidative stress and dismutates $\cdot O_2^-$ to H_2O_2 and oxygen. Catalase in peroxisomes also decomposes H_2O_2 to water and oxygen. TRX is also a protein induced by oxidative stress and is reduced via S-S binding of the substrate protein by two SH groups in TRX and acts on the H_2O_2 elimination system via peroxiredoxins. HO-1 is an inducible cytoprotective enzyme that catalyzes the initial and rate-limiting reaction in heme catabolism and cleaves prooxidant heme to form biliverdin with the release of carbon monoxide. Biliverdin is converted into bilirubin in mammals; both of these have been known to have very strong antioxidant activities.

ROS cause various forms of cellular damage. 4-hydroxy-2-nonenal (HNE) and malondialdehyde (MDA) are the peroxidation reaction products of lipids, and 8-hydroxydeoxyguanosine (8-OHdG) is the product of DNA base modification. These products serve as oxidative stress markers.

The Origin of ROS Production in HCV Infection

Then, where is the place for oxidative stress overproduction in the liver of hepatitis C patients? The core protein is mostly localized to the endoplasmic reticulum, but we and other groups have shown its localization to the mitochondria in cultured cells and transgenic mice [12]. In addition, the double structure of mitochondrial membranes is disrupted in hepatocytes of core gene transgenic mice. Evidence suggests that the core protein modulates some mitochondrial functions, including fatty acid β-oxidation, the impairment of which may induce lipid abnormalities and hepatic steatosis. In addition, the mitochondrion is an important source of ROS. In livers of transgenic mice harboring the core gene, increased ROS production has been observed [2]. A recent study found, via proteomic profiling of biopsy specimens, that impairment of key mitochondrial processes including fatty acid oxidation and oxidative phosphorylation and of the response to oxidative stress occurs in HCV-infected human liver with advanced fibrosis [13]. Therefore, it is probable that the HCV core protein affects mitochondrial functions since such pathogenesis is observed in both HCV core-transgenic mice and HCV-infected patients.

The recent progress in proteomics has opened new avenues for disease-related biomarker discovery. We performed a two-dimensional polyacrylamide gel electrophoresis (2D-PAGE) of mitochondria isolated from HepG2 cells stably expressing the HCV core protein and